Renewable Energy 133 (2019) 770–786

Contents lists available at ScienceDirect

Renewable Energy

journal homepage: www.elsevier.com/locate/renene

Energy storage based on $SrCO_3$ and Sorbents—A probabilistic analysis towards realizing solar thermochemical power plants

Laureen Meroueh [a, *], Karthik Yenduru [b], Arindam Dasgupta [c], Duo Jiang [d], Nick AuYeung [e]

[a] Department of Mechanical Engineering, Massachusetts Institute of Technology, Cambridge, MA 02139, USA
[b] Association of European Renewable Energy Research, Place du Champ de Mars 2, 1050 Brussels, Belgium
[c] Siemens Corporation, Corporate Technology, USA
[d] Department of Statistics, Oregon State University, Corvallis, OR 97331, USA
[e] Department of Chemical Engineering, Oregon State University, Corvallis, OR 97331, USA

ARTICLE INFO

Article history:
Received 5 July 2018
Received in revised form
3 September 2018
Accepted 15 October 2018
Available online 18 October 2018

Keywords:
Strontium carbonate
Thermochemical
Energy storage
Solar energy
Reversible CO_2 storage
Renewable energy

ABSTRACT

As greenhouse gases threaten our environment, it has become increasingly necessary to replace consumption of fossil fuels with renewable energy. Without energy storage, solar cannot provide power at night during times of peak demand, resulting in a gap between supply capabilities and demand. Solar thermochemical energy storage (TCES) has potential to resolve this critical temporal issue. An 800MWh_{th} TCES subsystem has been designed to cost-effectively convert solar energy to electricity. An evaluation of each required component is provided, including the reactor chemistry. Strontium carbonate decomposition is used to densely store high temperature thermal energy via chemical reaction, while two different CO_2 storage methods are considered. To determine the practical feasibility of these schemes, a probabilistic analysis has been performed to explore exergy and energy efficiency, and cost. It has been found that a scheme storing CO_2 via sorbents is capable of ~71% energy and ~87% exergy efficiency, and an installed cost of ~48 USD kWh_{th}^{-1}.

1. Introduction

With increasing need to harness intermittent renewable energy such as solar and wind, without threatening the stability of the electric grid, energy storage is imperative. It is expected that by the year 2020, over 26% of global power generation will be derived from renewable energy [1]. Although the adoption of photovoltaic (PV) systems has increased with the decrease in manufacturing cost, there remains the issue of producing energy when solar radiation is not sufficient as a result of geographic region, weather, or time of day. Therefore, cost-effective storage of electrical energy or an alternative to PV cells must be developed to provide a dispatchable source of energy.

From a storage perspective, solar thermal energy proves advantageous since there is inherently an intermediate step of converting heat to electricity, thus allowing for several storage options (sensible, latent, or thermochemical energy storage). Energy storage in the form of thermochemical energy offers the highest energy storage density compared to sensible and latent heat, by harnessing the change in enthalpy of chemical reaction, i.e. heat or enthalpy of reaction (ΔH). Through reversible reactions, such as $A + B \Leftrightarrow AB + \Delta H$ in which states A, B, and AB can vary, the energy of chemical processes can be harnessed for power production. A higher energy density allows smaller volumes of storage material and hence typically lower cost per kilowatt-hour. Such heat-driven chemical processes can be used to support solar-based power production. Although thermochemical energy storage (TCES) is a promising technique for enabling greater penetration of renewable energy into the power grid, solar energy power production coupled to TCES has yet to be sufficiently explored. To evaluate the feasibility of implementing a solar TCES subsystem, the system cost, energy efficiency and exergy efficiency must first be determined and compared to standards set by the US Department of Energy (DOE).

1.1. United States Department of Energy SunShot Initiative

The U.S. DOE has set targets for concentrated solar power and thermal energy storage systems to be met by the year 2020. Such targets consider both the economics and the efficiencies of the design. Along with the limits that the DOE has set, there are also

* Corresponding author.
E-mail address: laureenm@mit.edu (L. Meroueh).

https://doi.org/10.1016/j.renene.2018.10.071
0960-1481/

environmental and practical standards to meet. According to the DOE SunShot Initiative, the normalized cost of the energy storage subsystem must be less than \$15 kWh_{th}^{-1}. To achieve high exergetic efficiencies, the operating temperatures of the TCES processes must have temperatures greater than 650 °C. The SunShot Initiative criteria is based on the premise that a sufficiently high exergetic efficiency and high volumetric energy density will lead to a low normalized storage cost [2]. Furthermore, the energy storage system must be reversible and the selected TCES processes should not have undesirable side reactions, nor hazardous byproducts or leakage [3].

1.2. Solar reactor temperature versus efficiency

The solar receiver to be considered here consists of an aperture to which the concentrated solar flux from the heliostat field is directed. As the ratio of aperture diameter to length of the receiver approaches zero, the receiver approaches that of a blackbody absorber. Within the solar receiver, the concentrated sunlight is converted into heat, which is then used to drive the endothermic reaction within the thermochemical reactor. As all heat engines strive towards the Carnot efficiency, high temperatures are amongst the critical parameters of thermochemical systems. With respect to thermodynamics, an increase in temperature can result in an increase in energy efficiency, as seen in the basic Carnot efficiency equation $\eta = 1 - T_c/T_H$ where T_c is the temperature of the cold reservoir and T_H is the temperature of the hot reservoir relevant to the exothermic reaction. However, higher temperatures also contribute to radiant losses from the solar absorber, thereby reducing absorbed power. Thus, for thermochemical processes, the absorption efficiency and Carnot efficiency must both be considered in the following equation [4,5]:

$$\eta = \eta_{absorption} x\, \eta_{Carnot} = \left(1 - \frac{\sigma T^4}{IC}\right)\left(1 - \frac{T_C}{T_H}\right) \quad (1)$$

where T is the nominal cavity temperature, being the solar reactor in this consideration, σ is the Stefan-Boltzmann constant, I is the intensity of the solar radiation, and C is the mean solar flux concentration ratio. The chemical kinetics and heat transfer mechanisms concerning absorption, scattering, internal radiation-conduction, and re-radiation are complex processes that will not be detailed in this discussion, but can be found in the literature [4–7]. The main point to be made from Eqn. (1) is that in designing the solar reactor, the tradeoff between absorption and Carnot efficiency with respect to absorber temperature must be considered.

2. System description

Here, a solar TCES subsystem, capable of storing 100 MW of thermal power (MW_{th}) for 8 h, is designed with the goal of calculating total capital cost of the system. In describing system behavior, on-sun conditions refer to periods during daytime when solar radiation can be absorbed by the reactor. Off-sun conditions refer to periods when solar radiation is not available, i.e. during night-time or times of unfavorable atmospheric conditions. Hence, during off-sun conditions, the stored thermochemical energy must be released for power production. As an analogy to a typical electrochemical battery, charging refers to the period of time in which the system is "on-sun" carrying out the thermal decomposition of the selected TCES chemistry by absorption of solar energy within the reactor. Discharging can occur off-sun, or on-sun, and describes the stage at which energy is released by recombining the reacting materials.

Fig. 1 below depicts the overall system design of a typical power plant integrated with concentrated solar power (CSP) and a TCES subsystem. The following report will review the solar receiver-reactor with focus on the energy storage method and resulting components required for the selected energy storage method.

Ströhle et al. recently proposed a "bottom up" approach to designing CSP systems that utilize TCES, in which the gas-solid contacting pattern dictates the overall design. The TCES subsystem may be integrated with the power block through a parallel or serial configuration. A parallel configuration involves segregation of heat transfer processes between the solar field-power block and solar field-TCES subsystem upon charging of the TCES subsystem. For maximum efficiency, it would be desirable to have the working fluids exiting from both the TCES charging process and the power block exit at the same temperature. A series configuration couples the charging process of the TCES subsystem to the power block by utilizing the high temperature of the reactor upon charging to heat the HTF sent to the power block. During discharge, both concepts rely on the TCES subsystem for the energy to operate the power block. Depending on the chemical reactions and overall process design, heat integration may use one or more heat exchangers and one or more heat transfer fluids. To better simplify designs and gain higher effectiveness, some systems may make use of direct heat transfer between gas and solids [8]. In the case of the system proposed here, direct heating of solids by a solar field in a receiver-reactor is implemented rather than using a HTF.

Ströhle et al. also argued that particle size has a strong influence on the choice of reactor (e.g. packed beds, moving beds, fluidized beds, etc). Hence, solar reactor chemistries are compared first, with respect to ΔH, decomposition temperature, and resource abundance. Upon recommendation of $SrCO_3$ as the reactor chemistry, the appropriate reactor(s) are introduced. In order to utilize solar energy regardless of temporal and atmospheric conditions, the CO_2 from the decomposition of $SrCO_3$ must be stored efficiently to provide an exothermic reaction upon eventual re-entrance into a carbonation reactor. Two overall process flows have been devised, one including CO_2 storage in the form of compressed gas (Scheme 1) and the other including a reversible CO_2 absorption method (Scheme 2). To design for widespread adaptation, the system must prove efficient with respect to exergy, energy, and cost. A techno-economic analysis provides information on the magnitude of beneficial impact a technology or system can provide for its intended application, critical for determining the value of further pursuit. Thus, the performance of each Scheme has been evaluated and subjected to a Monte-Carlo based probabilistic analysis. By evaluating the technical and economic feasibility of a solar thermochemical energy storage subsystem, the following analysis aims to demonstrate how a solar-driven thermochemical energy storage subsystem for a generic power plant may be realized and encourage further research on the subject.

3. Results and discussion

3.1. Evaluation of solar reactor chemistries

A plethora of TCES chemistries have been studied and tested as viable solar reactor materials. The DOE requires these TCES processes to have operating temperatures above 650 °C and a high heat of reaction, along with the other standards previously stated. Given the capabilities of current concentrator technologies and the nature of available solar flux, the desired reaction temperatures for CSP applications fall within the range of 700–1100 °C [9]. Reaction chemistry can be characterized through the Gibbs free energy G, a function of pressure p and temperature T, defined as

$$G(p,T) = H - TS \quad (2)$$

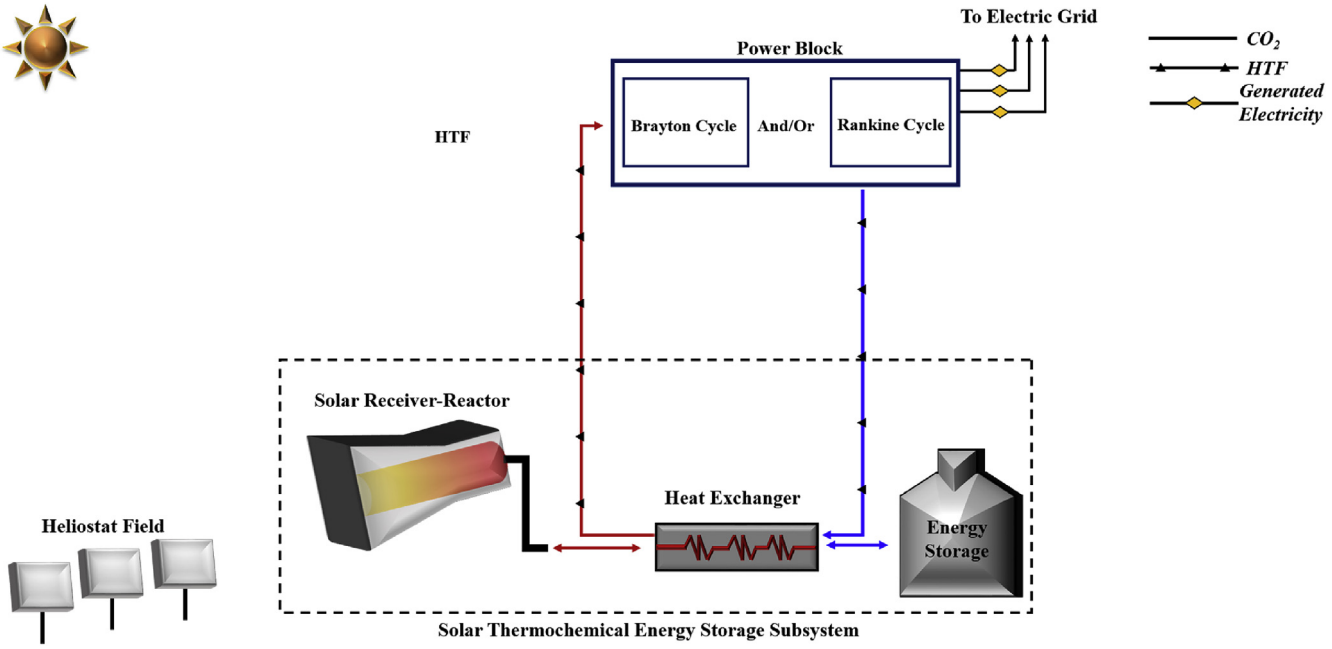

Fig. 1. Generalized layout of potential power block utilizing CSP and TCES.

The thermodynamic variable H is enthalpy, and S is entropy. At $\Delta G \cong 0$, the enthalpy must equate to the product of temperature and entropy. The generated entropy can be minimized by operating at high temperatures, according to $\Delta H/T_0 = \Delta S$, while maintaining a large enthalpy through the reaction. However, the temperature is limited to those within a practical range.

As candidates for TCES chemistries, there are gas-gas reactions and solid-gas reactions to consider. Typically, these reactions consist of thermal decomposition of a product for which the reactants are stored separately, then later recombined to release the enthalpy of reaction. Table 1 provides a comparison of such TCES processes that have been studied with respect to their enthalpy of reaction at standard pressure, ΔH_{rxn} at STP, and the corresponding temperature. Unlike most solid-gas reactions, metal hydride TCES systems use a high temperature solid and a low temperature solid to store/release the hydrogen, which can reduce system size and cost through higher energy densities in the storage process. When solar radiation is available, the high temperature metal hydride (HTMH) endothermically releases hydrogen, which is then stored in the low temperature metal hydride (LTMH). During times that solar radiation is not available, the reverse exothermic process occurs. Optimal HTMHs have a large enthalpy of reaction, high working temperature, high hydrogen capacity, and low raw material cost. Optimal LTMHs have a small enthalpy, low working temperature, high weight capacity, and low raw material cost [10]. A compilation of metal hydride properties is presented in Table 2.

Typical operating temperatures of a Brayton cycle are ~1200 °C. To minimize entropy generation, the working fluid of the solar TCES system should match closely to this temperature. Furthermore, higher temperatures within the solar receiver-reactor can lead to lower absorption efficiencies, as elaborated upon in the Section 1.2. At first review of the values provided in Table 1, Cs_2O and $SrCO_3$ appear to be the best candidates of the listed chemistries considering their high energy density and suitable operating temperature. However, Cesium is not available in commercial quantities and resources are limited, which will lead to prohibitively high cost [17]. As for the $SrCO_3$ chemistry, being the 15th most abundant element of earth, strontium mineral is readily available and inexpensive [18]. Along with being an abundant resource, $SrCO_3$ possesses a high energy density of 234 kJ/mol. In addition, the

Table 1
Comparison of TCES reactions.

Reaction	ΔH_{rxn} STP (kJ mole^{-1})	Temp (°C)	Ref.
Gas-Gas Reactions			
$NH_3 \leftrightarrow 3/2H_2 + 1/2N_2$	67	478	[11,12]
$2SO_3 \leftrightarrow 2SO_2 + O_2$	98	827	[12]
$NH_4HSO_4 \leftrightarrow NH_3 + H_2SO_4$	132	740	[12]
$CH_4 + H_2O \leftrightarrow 3H_2 + CO$	206	1012	[12]
$CH_4 + CO_2 \leftrightarrow 3H_2 + 2CO$	247	1012	[12]
Solid-Gas Reactions			
$MgH_2 + \Delta H \leftrightarrow Mg + H_2$ (g)	75	280	[13]
$Ca(OH)_2 + \Delta H \leftrightarrow CaO + H_2O$	109	507	[12]
$2CuO + \Delta H \leftrightarrow Cu_2O + ½\ O_2$(g)	143.1	1025	[12]
$CaCO_3 + \Delta H \leftrightarrow CaO + CO_2$ (g)	178	837	[12,14]
$CaH_2 + \Delta H \leftrightarrow Ca(g) + H_2$ (g)	181	950	[13]
$2Co_3O_4 + \Delta H \leftrightarrow 6CoO + O_2$	205	900	[15]
$SrCO_3 + \Delta H \leftrightarrow SrO + CO_2$ (g)	**234**	**1175**	[12,16]
$Cs_2O + \Delta H \leftrightarrow 2Cs(g) + ½\ O_2$(g)	481	1159	[12]
$Na_2O + \Delta H \leftrightarrow 2Na(g) + ½\ O_2$(g)	634	1607	[12]
$MgO + \Delta H \leftrightarrow Mg(g) + ½\ O_2$ (g)	752	3087	[12]

Table 2
Metal hydride properties selected for CSP application [10].

	Working Temp. (°C)	ΔH (kJ mol H_2^{-1})
HTMH		
MgH_2	300–500	75
Mg_2FeH_6	350–550	77
$NaMgH_3$	400–600	88
LiH	950–1150	190
$TiH_{1.72}$	650–950	142
CaH_2	900–1100	171
NaH	400–600	130
LTMH		
$TiFeH_2$	0–120	28
$TiCr_{1.8}H_{3.5}$	0–70	20
$TiMn_{1.5}H_{2.5}$	0–120	28
$NaAlH_4$(SAH)	80–120	40

temperature at which the Gibbs free energy of this reaction is at a minimum (i.e. $\Delta G \cong 0$) occurs at 1175 °C (at atmospheric pressure), which results in a very high quality of heat release, yet still in a practical temperature range. Among the listed chemistries, calcium carbonate ($CaCO_3$) is one of the most widely analyzed compounds for CO_2 capture and storage due to its relatively high operating temperature, high heat of reaction, and availability. However, in comparison to $SrCO_3$, $CaCO_3$ operates at a lower temperature, which will result in lower efficiencies.

In an analysis performed by Corgnale et al. [10], three HTMH candidates were selected based on cost, working temperature, volumetric energy density, and exergetic efficiency. The HTMHs deemed most attractive were then paired with LTMHs based on kinetics. These three were $NaMgH_3$ with SAH, $TiH_{1.72}$ with $TiFeH_2$, and CaH_2 with $TiFe_2$ [10]. In comparison to MH based systems, the $SrO/SrCO_3$ cycle has a higher energy density and higher working temperature than all three HTMHs. Furthermore, there are no side reactions present within the reversible strontium carbonate decomposition, nor a catalyst required, while MH reactions suffer from both.

Given the high energy density and the favorable characteristics of the $SrO/SrCO_3$ cycle as described above, the $SrO/SrCO_3$ cycle is the pursued TCES process for this subsystem design. Since small particles (e.g. 100 μm or less) have been used in previous $SrO/SrCO_3$ work [16], it is proposed that a fluidized bed be used for the carbonation step as part of a serial configuration. Fluidized bed combustion reactors allow for optimal gas-solid and solid-solid heat transfer—a critical characteristic for high rates of heat transfer within the solar thermochemical reactor [19,20]. The charging step can be carried out in a rotary kiln-type reactor which has seen solar implementation previously [14,21,22]. The rotary kiln allows for minimal radiation losses, improved heat transfer between gas and solid phase reactions, high reactive surface area, amongst other advantages presented in Appendix A.

The serial configuration enables heat to be extracted from the hot CO_2 stream exiting the reactor for use in power generation. Air would most likely be the working fluid, absorbing heat from carbonation and decomposition reaction. Admittedly, there are disadvantages in cost in using a separate rotary kiln reactor (during charging) and a fluidized bed reactor (during discharge). However, since the high temperatures involved require direct heating of the $SrCO_3$ material, a kiln is the best choice for coupling the reaction with the solar resource [8]. Additionally, CFB reactors can incorporate various heat exchanger designs within the reactor. To capture the heat released upon exothermic reaction, a plate heat exchanger or fluid bed heat exchanger, utilizing air as the heat transfer fluid (HTF), can be incorporated [23].

Both the decomposition reactor and carbonation reactor design largely depend upon the reaction kinetics of $SrCO_3$, which were unknown until recent [24]. Additionally, specific to the fluidized bed reactor, bed void fraction, internal porosity of particle, and gas-solid contacting pattern time [8]. While detailed design of a decomposition and carbonation reactor is beyond the scope of this paper, an overview of pilot-scale reactors is provided in the Appendix A. The extent of reaction for decomposition and carbonation vary depending on the partial pressure of species present in the system, precise knowledge of which would require analysis that is beyond the scope of this paper. Here, a base case is considered, in which 100% decomposition is achieved while roughly 50% of carbonation is achieved.

3.2. Process design schemes

Of the various possible Schemes applicable for a solar thermochemical subsystem based on the $SrO/SrCO_3$ carbonate chemistry, two preliminary Schemes have been selected for analysis. Scheme 1 describes a design in which CO_2 is stored as a pressurized gas without the use of a CO_2 ad/absorbent whereas Scheme 2 describes a design with the use of CO_2 ad/absorbent.

3.2.1. Scheme 1

Following Fig. 2a below, the first component in the processes is a solar reactor in which thermal energy, *Q*, from the solar heliostat field enters via radiation during the charging period. Through the absorption of *Q* within the reactor, the endothermic decomposition of $SrCO_3$ into SrO and CO_2 occurs. The high temperature SrO particles from the decomposition reaction are then stored in a thermally insulated storage tank as the CO_2 flows to a heat exchanger through which sensible heat of CO_2 is transferred to the HTF for utilization within the power block. It should be noted that the reactor and the subsequent heat exchanger could potentially be a coupled device, but are conceptually isolated here for purposes of illustration. Following the cooling of CO_2, the gas is compressed to 25 bar in preparation for storage. The final component in the charging process flow is the storage tank. During discharge, illustrated in Fig. 2b, CO_2 is released from the storage tank and is directed to the reactor. As higher pressures give rise to an increase in extent of reaction, the carbonation reactor is at a pressure 20 bar [16]. Given a pressure difference of 5 bar between the storage tank and reactor, the fluid may flow without necessitating the addition of a pump to the system. During the discharge process, SrO is also directed to the reactor from its corresponding storage tank. Within the reactor, the CO_2 exothermically recombines with SrO to form $SrCO_3$ during off-sun conditions, releasing energy commensurate to the enthalpy of reaction and molar volume of reactants. The carbonation temperature is 1150 °C, at which the SrO and CO_2 begin to exothermically recombine, giving rise to the reaction temperature heating up to 1235 °C. Finally, the heat released is captured via heat exchanger within the fluidized bed reactor and sent to the power block for electricity production. Fig. 2 also notes the thermodynamic properties of the CO_2 exiting each component.

3.2.2. Scheme 2

In Scheme 2, sorbents are used to capture the CO_2 rather storing it as purely pressurized gas, as considered in Scheme 1. Following Fig. 3a, the solar reactor, SrO storage vessel, and heat exchanger all behave the same way as described for Scheme 2. Unlike Scheme 1, the CO_2 is now stored via reversible ab/adsorption at closer to atmospheric pressure, potentially leading to lower cost. During discharge, Fig. 3b, the CO_2 is released from the selected sorbent in the storage vessel. The method of CO_2 release is highly dependent upon the type of material chosen for reversible CO_2 capture, and is further described in the following section concerning reversible CO_2 storage evaluation (section *4.4*). The discharged CO_2 is then compressed to 25 bar via a compressor and directed to the carbonation reactor.

3.3. Reversible CO_2 storage materials

The most applicable and practical CO_2 ad/absorption materials have been evaluated. The quantitative results are presented in Table 3, including their operating pressure (*P*) and temperature (*T*). A detailed literature review of reversible CO_2 capture methods is presented in the Appendix B, along with an elaboration of estimation methods for values presented in Table 3.

There are two main parameters to which the listed materials in Table 3 should be compared: total cost per unit energy stored and the regeneration penalty (q_R) at a corresponding temperature (T_R), which will lower the energy and exergy efficiency. The total cost listed includes the raw material cost for the substance and the

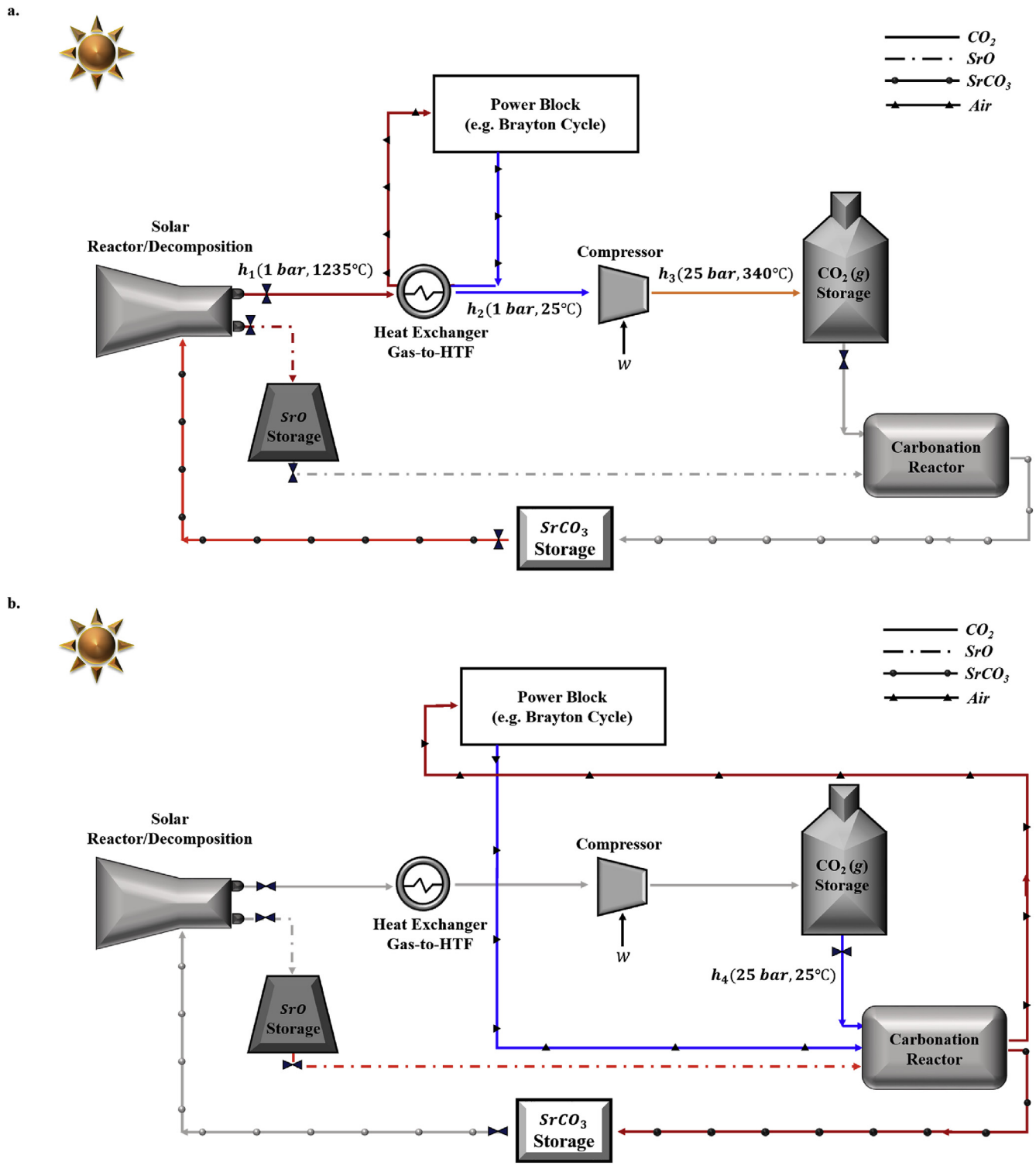

Fig. 2. Solar Thermochemical Energy Storage Subsystem, Scheme 1, during (a) on-sun operation and (b) off-sun operation. Scheme 1 does not use a solvent or sorbents to capture the evolved CO_2. Rather, the CO_2 is compressed to 25 bar and stored in a tank. During discharge, the CO_2 is released from the storage tank and flows to the carbonation reactor for power production.

storage tank cost, details of which are included in the Table B.1 of Appendix B. Not included were the costs of additional compressors or heat exchangers, if needed.

Given the low amount of energy input required and low cost per kWh_{th}, activated carbon (AC) proves to be an attractive reversible CO_2 storage method. Specifically, AC CS-6-CD-8 is the more suitable of activated carbons with respect to cost and adsorption capacity. As displayed in Table 3, AC CS-6-CD-8 has a calculated normalized cost of \$3.19 per kWh_{th}. However, this cost corresponds to AC at 0 °C, therefore necessitating an additional cost to cool CO_2 to a temperature (T) of 0 °C, versus 25 °C. Another viable option for a reversible CO_2 storage method is the ionic liquid [Cho][*p*-methoxy-

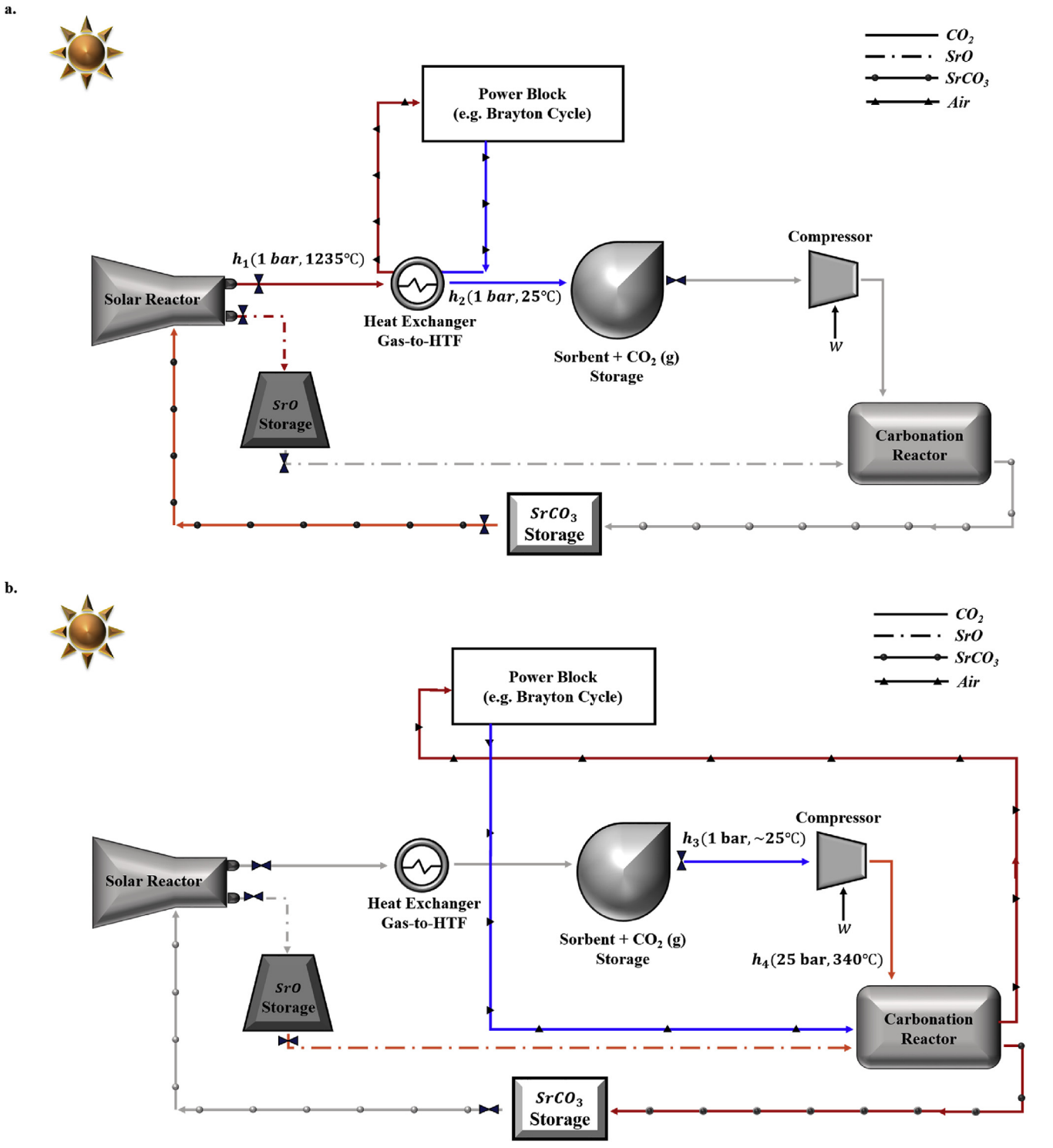

Fig. 3. Solar Thermochemical Energy Storage Subsystem, Scheme 2, during (a) on-sun operation and (b) off-sun operation. Scheme 2 depicts the processes included in one of the two considered solar thermochemical subsystem designs, which does use a solvent or sorbents to capture the evolved CO_2. While the sorbent remains within the storage tank during both charging and discharge, the CO_2 is released from the sorbent and storage tank during hours of discharge. Compared to Scheme 1, the compressor is now located after the storage tank rather before.

PhO]. This ionic liquid has attractive recyclability characteristics and a low reported cost of \$2.14 per kWh_{th}. The only potential deterrent to using this ionic liquid would be the enthalpy of absorption, a currently unknown value. A noticeably lower cost of \$0.13 per kWh_{th} was achieved by CO_2 stored as a solid. However, this storage method requires gaseous CO_2 to undergo energy intensive cooling and/or compression to reach the adequate temperature and/or pressure (P) before reaching its solid phase. This cooling process of CO_2 from a gas at 25 °C to a solid at −70 °C entails an additional cost to the system. Storing CO_2 at ambient temperature, under pressure to reduce volume, is an option less energy demanding than solid CO_2, yet still requires the further work input

Table 3
Evaluation of reversible CO_2 storage methods.

Substance	(P[a],T)	Energy Density (kWh_{th}/m^3)	q_R (kJ/mol)	T_R	Total Cost ($ kWh_{th}^{-1})
[Cho][p-methoxy-PhO] [25,26]	(1, 30 °C)	263.16	19.1–89.9	–	$2.14
DES ChCl:Gly:SB [27]	(1, 25 °C)	551.72	–	–	$2.47
AC CS-6-CD-8 [25]	(1, 0 °C)	467.84	22.9–26.5	0 °C	$3.19
AC CS-6-CD-4 [25]	(1, 0 °C)	547.95	20.3–27.7	0 °C	$3.37
Amine PZ/DETA/$H_2$0 [28]	(-, 50 °C)	754.72	145.02	120 °C	$3.67
Sorbent K_2CO_3/MgO [29]	(1, 60 °C)	583.94	236	400 °C	$3.75
Amine PZ/DETA/MeOH/H_2O [28]	(-, 30 °C)	588.24	102	120 °C	$3.92
AC CS-6-CD-4 [25]	(1, 25 °C)	331.95	20.3–27.7	25 °C	$5.49
AC CS-6-CD-8 [25]	(1, 25 °C)	255.59	22.9–26.5	25 °C	$5.73
Sorbent K_2CO_3/AC [29,30]	(1, 60 °C)	280.70	89.5	150 °C	$9.10
$Ba_4Sb_2O_9$ [31]	(-, 600 °C)	567.38	156	950 °C	$14.72
Gas	(1, 25 °C)	0.59	N/A		$225.35
Pressurized Gas	(25, 25 °C)	14.67	N/A		$66.79
Solid	(1, −78.5 °C)	2305.48	N/A		$0.13

[a] In units of bar.

to the compressor and a high pressure vessel. After evaluation of the various CO_2 storage methods with respect to cost and efficiency, it appears that storing CO_2 through ab/adsorption is more effective than storing CO_2 as a gas.

3.4. Cost analysis

3.4.1. Cost estimate of major subsystem components

The purpose of this paper is not to perform a detailed design of a solar TCES subsystem but rather, to estimate the cost and efficiency of a solar TCES subsystem to help determine whether such a system is a feasible alternative to fossil-fuel fired plants. As such, the major subsystem components are designed with the main goal being a cost estimate of the component. As the purpose of this study is to determine whether solar TCES can be practical and cost-effective, the total system cost must account for costs beyond raw materials. Therefore, delivery and installation costs are factored into the total normalized cost of the thermochemical subsystem, under base case conditions of 50% extent of carbonation. Due to the preliminary nature of this study, a rigorous design of a carbonation reaction (e.g. a fluidized bed) and solar receiver-reactor for decomposition is not performed here.

To estimate purchased equipment cost of the major subsystem components, the following cost correlation was used

$$C_e = a + bS^n \tag{3}$$

where a and b are cost constants that depend on the type of process, n is an exponent dependent upon the type of equipment, and S is a size parameter of the component [32]. The total capital cost is calculated by summing the capital cost per piece of equipment, which includes piping, insulation, painting, equipment erection including foundations, instrumentation, and material factors through a total installation factor, *IF*. The installation factor is calculated through Eq. (4) and the installed cost per piece of equipment, C, is calculated through Eq. (5) [32].

$$IF = \left(1 + f_{piping}\right) f_{material} + \left(f_{erection} + f_{instrumentation} + f_{insulation}\right) \tag{4}$$

$$C = C_e \cdot IF \cdot \frac{CE\ index\ 2014}{CE\ index\ 2010} \tag{5}$$

In Eq. (4), f is the installation factor corresponding to the piping, material, equipment erection, instrumentation, and insulation. Values for the installation factors were taken from Towler and Sinnott. The Chemical Engineering Plant Cost Index (CE index) accounts for cost inflation and is used to estimate the cost of a piece of equipment for which the past price is known [32]. The CE index of 2010 and 2014 are used to predict the equipment cost in 2014, given pricing from 2010.

The authors of this paper have previously shown decomposition $SrCO_3$ and extraction of CO_2 at 1235 °C. Hence, the following calculations assume that the SrO and CO_2 exiting the solar heated rotary kiln are at 1235 °C [16]. In estimating the cost of a rotary kiln, a simple sizing exercise is first performed for a cylindrical vessel. A 316 stainless steel casing is considered, internally lined with aluminosilicate insulation to handle the high temperatures of ~1235 °C. The internal pressure of the rotary kiln is 1 bar, corresponding to the decomposition pressure. Nominally, each reactor will be subject to a solar flux of ~1 MW/m^2. Hence, for a solar TCES subsystem capable of 100 MW_{th}, there can be 8 solar reactors each with an internal radius of 2 m, resulting in an installed cost of $6.29/$kWh_{th}$. A smaller or larger internal radius results in a cost increase due to the interplay between radius and number of reactors for a given power requirement. Further details of the rotary kiln reactor design are included in Appendix C. For a detailed design of a rotary kiln, more accurate and optimized dimensions must be calculated along with specific residence time with respect to the actual reaction rate, as previously done by Tescari [33,34].

For the storage of solids (i.e. SrO and $SrCO_3$), a cylindrical cone-roof tank and floating roof storage tank are considered. The volume of the SrO and $SrCO_3$ storage tanks are commensurate to the amount of solids needed for achieving 800 MWh_{th} of storage, with factors accounting for void space ratio, extent of reaction for thermal decomposition and carbonation, and the mass flowrates of $SrCO_3$ and SrO. The void space for solid storage ranges between 40 and 50% of total volume for most cases, and higher for increased particle size [35]. Here, a conservative void space (ϕ) of 50% is considered. Storage tank volume (V) for substance x, SrO or $SrCO_3$ in this case, can then be calculated as

$$V_x = \left(\frac{MW_x}{\rho_x}\right) \frac{1}{\phi \eta_c} \frac{Qt}{\Delta H} \tag{6}$$

where MW is molecular weight, ρ is gravimetric density, η_c is the carbonation efficiency, Q is the power rating, and t is storage duration in seconds. Using cost correlations as shown in Equation (3), the total installed cost per insulated cone-roof storage tank for SrO and $SrCO_3$ is $1.77 $kWth^{-1}$. It must be noted that these values for storage tank volume are subject to change based upon the amount of dopants needed to prevent sintering for the particular reactor chemistry considered.

During charging, as the SrO is directed to the high temperature

storage tank, CO_2 must pass through a gas-gas high temperature heat exchanger to be cooled and stored at ambient temperature. In this case, air is considered as the working fluid for the power block. Hence, CO_2 enters the heat exchanger at 1235 °C and exits at 25 °C, transferring heat to air that is then sent to the power block. The pressure of the CO_2 exiting the reactor is assumed to be at atmospheric pressure, while the pressure of the cooling fluid is assumed to be around 20 bar. The heat exchanger area can be determined by relating the first law of thermodynamics to the overall heat transfer equation for a single pass heat exchanger, as shown in Appendix C.

A ceramic heat exchanger is able to handle the high CO_2 temperature of 1235 °C exiting from the reactor, albeit at a high capital cost around \$11.80 kWh_{th}^{-1} for commercially available equipment as estimated by Heat Transfer International Co. This cost considers both the sensible heat from the charging process and enthalpy of reaction from discharging process. For comparison, the cost of a low temperature stainless steel HX was calculated, which would no longer capture the sensible heat from the charging process. A low temperature gas-gas shell and tube heat exchanger is considered, of the floating head type, with the concession that the energy and exergy efficiencies would decrease. The floating head shell and tube heat exchanger allows for large heat transfer surface area, necessary to compensate for the low heat transfer coefficient between gaseous fluids [36]. The resulting purchased cost is approximately ~\$3.02 kWh_{th}^{-1}. The considerable difference between heat exchanger price as a function of fluid temperatures leads to the unavoidable tradeoff between performance and cost which arises in most systems. It should be noted that further development and economies of scale may significantly decrease the capital costs of high temperature ceramic heat exchangers in the future. Additionally, a heat exchanger cost reduction of 40% is expected with 100% decomposition extent of reaction.

In Scheme 1, the CO_2 is compressed prior to the storage tank during the charging step whereas in Scheme 2, the CO_2 is compressed after exiting the storage tank during the discharging step. In determining the cost of the compressor, adiabatic and reversible compression (i.e. isentropic compression) of an ideal gas is assumed. Drive power, which is the characteristic value in the cost correlation, is calculated by determining reversible work done (W_{rev}) by the compressor as follows

$$W_{rev} = \left(\frac{k}{k-1}\right) P_1 V_1 \left[\left(\frac{P_2}{P_1}\right)^{\frac{k-1}{k}} - 1\right] \quad (7)$$

In which k for CO_2 is 1.29, P_1 and V_1 are the pressure and temperature of the CO_2 at the compressor inlet, respectively, and P_2 is the CO_2 pressure at the outlet. Further detail in calculating the reversible work is provided in Appendix C. The total installed cost of the compressor is estimated to be \$9.62 kWh_{th}^{-1}.

During discharge, CO_2 and SrO are both sent to a fluidized bed reactor in which they exothermically recombine, and that heat of reaction is captured by air flowing through the tubes in the fluidized bed. Due to the preliminary nature of the study, a rigorous fluidized bed design is not performed here. Auxiliary equipment costs are assumed to be included in the multiplication (i.e. Lang) factors. The general approach in sizing and costing the fluidized bed was to determine the necessary reactor volume and the corresponding cost of the vessel at the given pressure (20 bar). The pressure vessel is assumed to have fully radiographed double butt welds for a welded joint efficiency of 1.0. Due to the high temperatures and chemical environment, a corrosion allowance of 4 mm is added. Next, the heat transfer rate, which was assumed to be nominally 100 MW_{th}, was used to determine an approximate heat transfer area to use for costing the heat exchange portion. The sum of the vessel and heat exchanger costs are taken to be the estimated cost of the fluidized bed. Due to the uncertainty in the fluidized bed design, a highly conservative factor of 2 is included in the cost estimate. This results in a total installed cost of \$7.18 kWh_{th}^{-1}.

3.4.2. Probabilistic cost analysis

A probabilistic analysis on the total installed cost for both Scheme 1 and Scheme 2 subsystem has been performed, to account for uncertainty and variability in the values collected. The probabilistic analysis is based on Monte Carlo simulations with costs varied according to a Gaussian distribution. The price of $SrCO_3$ is subject to variation every year since it is either mined or imported. Strontium carbonate is the principal compound of strontium, with an imported cost of roughly \$0.82 per kg as of 2013 [37]. To account for this variable in a design that is expected to have a long lifetime, a ±30% cost variation in $SrCO_3$ was considered. The cost of pressurized CO_2 storage was also varied by ±30%. The possibility of different sorbents being used in Scheme 2 is reflected in this study by using the average and standard deviation of sorbent costs (ref. Table 3) in the probabilistic analysis.

The external factor applied in the installed cost calculations is defined as $\sum[C_e \cdot (IF - 1)]$, summed over all components. This results in a rigorous and conservative estimate of external factors as 110%–128% of the purchase cost, compared to assumed values of 10–15% in other techno-economic studies of similar applications [38,39]. To account for such a gap between estimated values in literature and the calculated values presented in this paper, the external multiplication factor was varied from 0.1 to 1.3 in the probabilistic analysis.

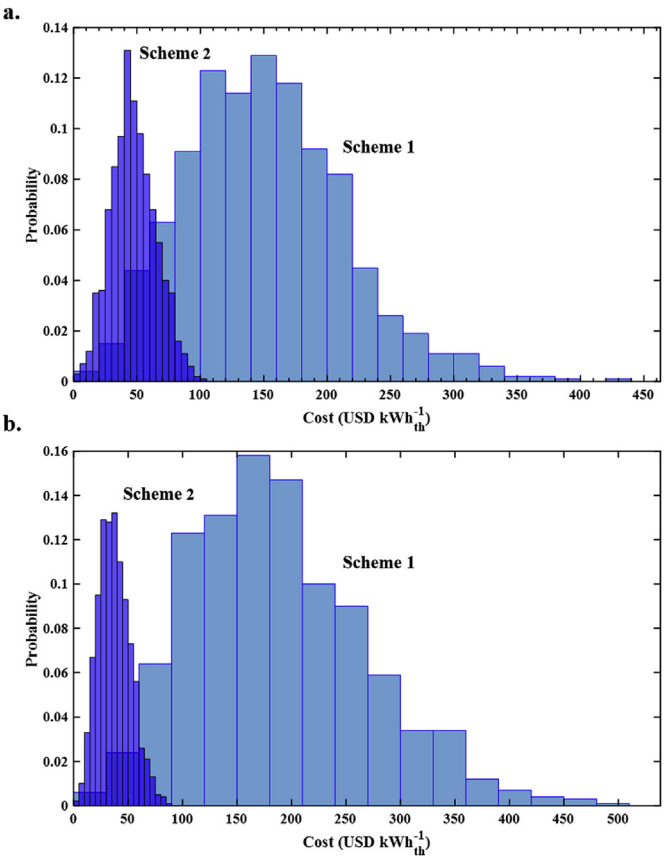

Fig. 4. Probabilistic cost analysis of each Scheme. (a) Considers high temperature heat exchanger and captured sensible heat. (b) Considers low temperature heat exchanger without the ability to capture sensible heat. Sample size of 1000 was implemented, for which variance of did not significantly affect the results of this cost analysis.

The results of the probability analysis (see Fig. 4) indicate that when including a high temperature heat exchanger that can capture the high temperature CO_2 exiting the reactor, a capital cost of 153±64 USD kWh_{th}^{-1} for Scheme 1 and 48 ±18 USD kWh_{th}^{-1} for Scheme 2 can be expected. For the case in which a less expensive low temperature heat exchanger is used, for which the sensible heat of CO_2 is no longer captured but lost, the probability analysis concludes in a capital cost of 185±81 USD kWh_{th}^{-1} for Scheme 1 and 39 ±16 USD kWh_{th}^{-1} for Scheme 2.

This analysis indicates that a solar TCES subsystem cost, excluding the cost of operation and maintenance, can be considerably more affordable when utilizing sorbents in the storage of CO_2. A slight cost reduction can further be achieved by using a low cost, low temperature heat exchanger, though this will reduce efficiency. Clearly, the configuration following Scheme 1 is prohibitively expensive and will require significant cost reductions to serve as a practical option for a solar TCES subsystem.

3.4.3. Cost reduction strategies

Since the main cost in Scheme 1 is the storage vessels, methods for decreasing said cost are analyzed. Fig. 5 displays the cost variation of CO_2 storage under increasing pressure (Scheme 1) and the exergetic efficiency with increase in pressure. Increasing pressure of the gaseous CO_2 reduces storage volume but also necessitates vessels with higher operating pressure rating. Exergetic efficiency will decrease with an increase in compressor work, as can be seen in Fig. 5.

The storage of CO_2 as a pressurized gas does not present itself as an economically viable option. The costs of compressors and high pressure vessels are unavoidable. Such conclusions have been confirmed widely, thus motivating research on low cost CO_2 absorbents and adsorbents, mainly for the purpose of reducing CO_2 emissions [28,40–45].

For Scheme 2, the main advantage of increasing pressure would be reduction in required volume of sorbent, thereby reducing overall system cost. An increase in adsorption density with increasing pressure has been experimentally supported by Himeno et al. specifically for activated carbons [46]. Sorbents such as activated carbon can even have an exponentially increasing CO_2 uptake with pressure [25]. This increased adsorption density will result in reduced raw material cost of the sorbent itself. However, the cost of the pressure vessel and compressor will increase with increasing pressure. Future work will consist of detailed sorbent volume versus pressure analysis to determine how significant the cost reduction can potentially be.

3.4.4. Payback period

A simple payback period is calculated based on the fixed capital investment, which includes field costs, installation labor and supervision, offside modifications to infrastructure, engineering cost, and contingency. The average annual cash flow is estimated based on the average retail cost of electricity (p) in the US for 2016, ~11 cents kWh_e^{-1}, the annual amount of electricity delivered by the TCES, and the annual costs incurred by the plant, i.e. O&M [47]. The calculated O&M for Scheme 1 is 22.76 USD kWh_{th}^{-1} while Scheme 2 has a much lower O & M cost of 4.70 USD kWh_{th}^{-1}. Details of operations & maintenance calculations are included in Appendix C.

To calculate simple payback period, a total investment cost is assumed to include the total fixed capital cost and working capital cost. Complete charge and discharge of the TCES subsystem is assumed on a daily basis, for every day of the year, resulting in an annual power production of $(Q/\eta_{PB}\eta_{TCES})\cdot t\cdot 365$ derived from the TCES subsystem. Here, Q is 100 MW, η_{PB} is the thermal-to-electric efficiency of the power block, η_{TCES} is the efficiency of the TCES subsystem, and t is the discharge duration of 8 h. The efficiency of the power block is assumed to be 60%, as is typically achieved in combined cycle power plants, with an efficiency of 70% considered for the TCES subsystem.

Fixed capital cost includes inside battery limits capital cost (TCC), outside battery limits (OSBL), engineering cost and contingency charges. The engineering cost includes cost of detailed design, construction supervision, and general administrative charges. Contingency charges are included to account for variation from the cost estimate, allowing for a more realistic estimate. Engineering cost and contingency charges are based on the ISBL and OSBL.

Due to the prohibitively high O&M cost for Scheme 1, calculated in Appendix C, the annual income would not compensate enough for the investment and expenses of the subsystem to result in a reasonable payback period. Hence, Scheme 1 has been excluded from the evaluation of simple payback time.

Upon calculation of the fixed capital, the payback period (N) is estimated as.

$$N = \frac{\text{Fixed Capital}}{p\cdot\frac{Q}{\eta_{PB}\eta_{TCES}}\cdot t\cdot 365 - O\&M} \tag{8}$$

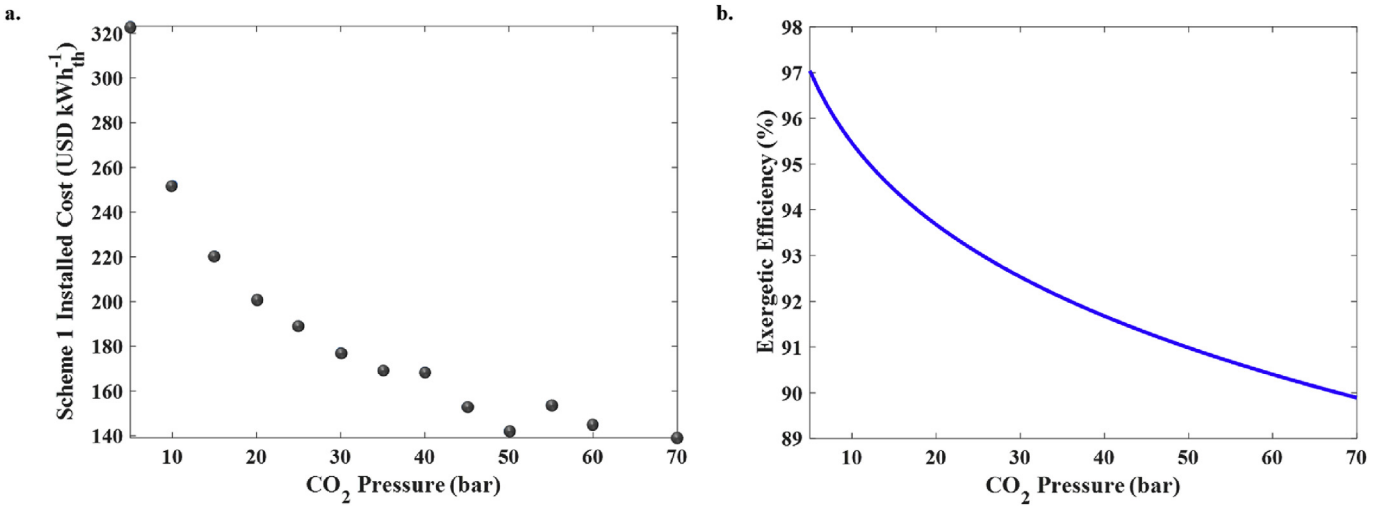

Fig. 5. Analysis of Scheme 1 (a) installed cost and (b) exergetic efficiency with increasing pressure of stored gaseous CO_2.

With all variables defined previously and values per variable provided in Table 4. The resulting payback period calculated for Scheme 2 is ~6 years, compared to the ~30-year lifetime of a typical power plant.

3.4.5. Open-scheme cost analysis

Incorporating CO_2 storage in a power generation system could also be achieved in an open system. Capture of flue gas from coal-fired power plants is a necessary subject of research to reduce carbon emissions, and has been explored via the use of sorbents, several of which are included in Section 3.3 and Appendix B [10,45,48–53]. A cost analysis of an open Scheme including a compressor and sorbent, considering storage of 25×10^3 kmol of CO_2 derived from the emissions of the power plant, is performed. Such a CO_2 storage system results in a total installed cost of 13.6 USD kWh_{th}^{-1}. Cost may be reduced further by considering storage of CO_2 under pressure in a sorbent such as activated carbon [46].

From a less environmental and more economic perspective, the CO_2 emissions from coal-fired power plants can also be used to generate heat in another open system design. Flue gas from the power plant may be sent to the carbonation reactor to exothermically react with SrO, thereby producing heat to be utilized by the existing power block. Decomposition of the $SrCO_3$ may be performed within the solar reactor utilizing solar radiation during on-sun period, and releasing the CO_2 into the atmosphere. Such an open system, consisting of the solar reactor, carbonation reactor, solids storage, compressor, and heat exchanger, would have an installed cost of 28.50 USD kWh_{th}^{-1}, assuming a conservative 50% thermal to electric efficiency of a combined cycle power plant with a gas turbine inlet temperature of ~1100 °C [54].

3.5. Exergy and energy efficiency

Based on the aforementioned design considerations, both Schemes have been evaluated from an exergy and energy perspective [55–57]. In order to accurately compare both systems, baseline assumptions were made. The overall exergetic efficiency considers the sum of irreversibilities identified per component. Scheme 2 consists of the same components as Scheme 1, with the addition of energy input to release the CO_2 from the sorbent. Discharging exergy also assumes complete discharge of CO_2, a variable that is subject to sorbent material and/or sealing of pressurized gas tanks/piping.

The exergetic efficiency of the heat exchanger is assumed to approach 99% efficiency in accordance with U.S. Department of Energy guidelines. Additionally, the exergy of the compressor (B_c) is assumed to be equal to the work input, i.e. $B_c = W_{rev}$ [2].

The energy input of the solar reactor is assumed to be 194.89 kJ/mol, equal to the enthalpy of decomposition of $SrCO_3$ at 1235 °C. Similarly, the energy output during off-sun conditions is 197.85 kJ/mol, equal to the enthalpy of carbonation at 1150 °C. Compressor work was calculated as previously shown in Equation (6), resulting in an energy input of 11.7 kJ/mol. High efficiencies can be realized with the inclusion of a high temperature heat exchanger, as considered in this analysis. Exergy due to carbonation, decomposition, and desorption are all calculated according to

$$B_{Q_i} = Q\left(1 - \frac{T_o}{T}\right) \tag{9}$$

where Q is the heat input or output, T is the corresponding temperature of operation, and T_o is the ambient temperature of 25 °C [2].

For Scheme 1, the resulting energy and exergy efficiency were determined to be 96% and 93%, respectively. Unique to Scheme 2 is the additional energy input required for regeneration of CO_2 from the chosen sorbent. The sorbents considered in the exergy and energy analysis were chosen based on regeneration temperature and required heat of regeneration. Included in the analysis are the amines PZ/DETA/H_2O and PZ/DETA/MeOH/H_2O, activated carbons CS-6-CD-4 and CS-6-CD-8 operating at 25 °C, and the Sorbent K_2CO_3/AC. Although the ionic liquid [Cho][*p*-methoxy-PhO] is highly attractive for its low cost and sustainability, the regeneration penalty is unknown. For regeneration temperatures around 150 °C and below, the required heat for CO_2 release can be directed from the main power block with potential of being waste heat i.e. cogeneration. However, other methods of release are viable which can increase exergetic efficiency, including electric swing adsorption, pressure swing adsorption, stripping technology, etc. [58].

To account for the sorbent selection flexibility and the inherent uncertainties of the sorbents still in research phase, the sorbent-dependent variables have been varied in the probabilistic analysis. A probabilistic analysis has been performed varying both enthalpy of desorption and temperature of desorption according to a Gaussian distribution, based on the sorbents considered. Monte Carlo simulations were performed in which values for the varied parameters were selected independently and randomly from the distribution. Results are shown in Fig. 6. According to a Gaussian distribution, an energy efficiency of 71%±12% can be expected with an exergetic efficiency of 87%±6%.

4. Conclusions

Strontium carbonate is capable of decomposing and carbonizing at very high temperatures, thus having potential for high heat-to-electricity conversion efficiencies for solar thermal power generation. The high energy density minimizes the reaction material required and thus further reduces cost. Strontium is also a widely available mineral within the crust of the earth, leading to an abundance of strontium carbonate at low price. To solve the problem of intermittency, CO_2 from the endothermic decomposition of SCO_3 via concentrated solar power is stored as either

Table 4
Scheme 2 Simple payback time estimated values.

Cost Variable	Calculation Method	Scheme 2 Cost
TCC	Equation 9	37 MMUSD
OSBL	40% of TCC	15 MMUSD
Engineering Cost	1% of (TCC + OSBL)	525,000 USD
Contingency	10% of (TCC + OSBL)	5.25 MMUSD
Fixed Capital	Fixed Capital = Σ(listed variables)	58.3 MMUSD
Working Capital	15% of Fixed Capital	8.7 MMUSD
Total delivered electricity from TCES subsystem	Based on 42% thermal-to-electric efficiency ($\eta_{PB}\eta_{TCES}$)	122,640 MW h yr^{-1}
O&M	(ref. Appendix C)	2.66 MMUSD yr^{-1}
Net Annual Income	Denominator of Equation (8)	9.7 MMUSD yr^{-1}
Simple Payback Time		**6 years**

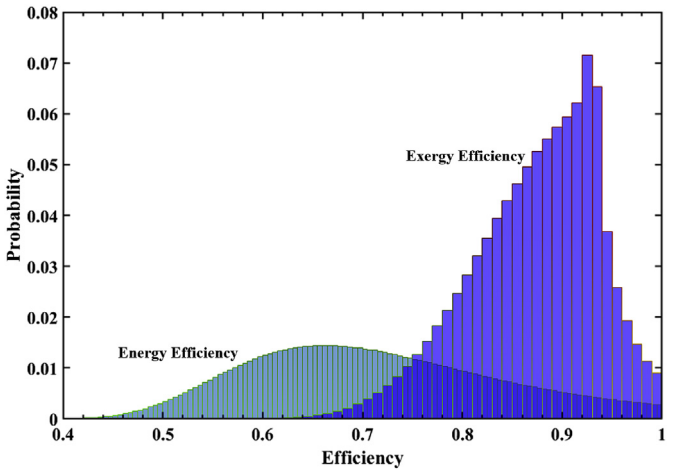

Fig. 6. Probabilistic analysis of exergy and energy efficiency achievable by Scheme 2 in which sorbents are utilized for CO_2 storage. Sample size of 2,000,000 was implemented, variance of which did not significantly affect results.

pressurized gas or by using a reversible CO_2 absorption method, several of which have been reviewed here.

An upper bound exergy analysis was performed for Scheme 1, resulting in an energy and exergy efficiency of 96% and 93%, respectively. To allow for flexibility in sorbent selection and account for uncertainty in sorbent thermodynamic properties, Monte Carlo simulations were performed, assuming some degree of normality with Gaussian distributions assigned to the enthalpy and temperature of desorption. An energy efficiency of 71%±12% and exergetic efficiency of 87%±6% is found to be most probable for Scheme 2. The main source of efficiency reduction in Scheme 2 compared to Scheme 1 is the heat of sorption required to regenerate the CO_2 from the sorbent. To better compare CO_2 stored under pressure versus CO_2 stored in a sorbent with respect to efficiencies, component-specific work focused on the storage method should consist of a more rigorous efficiency versus pressure calculation.

Additional probability analyses were performed to evaluate the cost of both Scheme 1 and Scheme 2. For a solar TCES subsystem using a high temperature ceramic heat exchanger to capture the sensible heat of the high temperature CO_2 exiting the reactor, it is found that a capital cost of 153±64 USD kWh_{th}^{-1} for Scheme 1 and 48 ±18 USD kWh_{th}^{-1} for Scheme 2 is most probable. Although the total capital cost of Scheme 1, in which CO_2 was stored as pressurized gas at 25 bar, far exceeds the goals set by the U.S. DOE, Scheme 2 has the potential to meet the \$15 kWh_{th}^{-1} requirement. In Scheme 1, regardless of increasing the CO_2 storage pressure in effort to reduce storage tank volume, the cost per kWh_{th} is still shown to greatly exceed that of Scheme 2. It is concluded that storing CO_2 as a pressurized gas does not behoove the overall economics of a TCES plant. Rather, storing CO_2 through physisorption or chemisorption may be the key to realizing affordable solar TCES power plants. A further decrease in Scheme 2 may be achieved by considering storage of CO_2 in a sorbent under pressure. Activated carbons have the ability to absorb CO_2 under pressure, and thus should be explored for this potential [46].

In order to meet the U.S. DOE targets, future work must be done to more accurately estimate the costs of the storage tank, compressor, external factors such as installation and delivery, and the heat exchanger. Chemistries that do not require gas storage (e.g. cycles that use air) or open-system CO_2-based chemistries may have advantages due to elimination of the CO_2 storage aspect. Further techno-economic process optimization must also be performed in attempt to reduce the cost of each individually designed component, considering the estimates and design calculations that the costs are based on were quite preliminary, with focus on storage tanks and high temperature heat exchangers. With the current crude estimates, it was determined that the \$15 per kWh_{th} target set by the U.S. Department of Energy is challenging. For any TCES chemistry, the longevity and regeneration costs of the reactive materials must be well studied. Nevertheless, high exergetic efficiencies are capable of achievement through this solar thermochemical storage subsystem design, and the cost for Scheme 2 has potential for improvement. Low temperature heat exchangers should be considered, at the cost of efficiency. Future work must be performed to determine the specific reaction kinetics of the SrO/$SrCO_3$ cycle, sorbent CO_2 storage material optimization, as well as a more tailored and detailed cost analysis.

Author contributions

Conceptualization, all authors; Calculations, L.M., N.A., K.Y.; Writing – Original Draft, L.M.; Review & Editing, all authors; Visualization, L.M.; Funding Acquisition and Supervision, N.A.

Appendices

Appendices include review of solar reactor technologies (Appendix A), review of reversible CO_2 storage technologies and Supplemental table with detailed cost analysis of various reversible CO_2 storage technologies (Appendix B), Cost and Design calculations of subsystem components (Appendix C), and three supplemental figures.

Acknowledgments

This work was supported by U.S. Department of Energy SunShot Initiative award DE-EE0006534.

Appendix A. Solar Reactor Technologies

Various reactors have been designed in effort to support industrial processes with solar thermal energy, while several of these have been developed to the pilot scale. The most popular reactor designs are that of rotating reactors, including the solar heated rotary kiln and the Zirrus reactor based on the Roca reactor which was designed for thermal reduction of ZnO, and the fluidized bed type, some of which have reached the on-sun pilot-scale testing phase [21,59–61]. There are reactor concepts that are currently under research at facilities such as PROcédés Matériaux et Énergie Solaire, Center National de la Recherché Scientifique (PROMES-CNRS) and Paul Scherrer Institut (PSI) amongst others. The following reactors to be mentioned are still at pilot scale with the exception of rotary kilns.

Roca Reactor

The ROCA reactor was the first to be conceptualized and constructed for experimental analysis. The first of reactors to be designed and subjected to experimental analysis, the ROCA reactor has been tested for thermal reduction of metal oxides such as ZnO (s), Fe_3O_4 (s), mixed iron oxides and Mn_2O_3 to a maximum temperature of 2000 K. Similar to ROCA with respect to purpose, reactor CAIRO was designed to gain further insight on thermal reduction kinetics of mixed iron oxides and mixed wustites [59]. However the reaction mechanism of CAIRO is fundamentally different from ROCA, as CAIRO imposes a constraint on particle size such that the reactant material is suspended with auxiliary gas (i.e. heat transfer fluid). This suspension efficiently absorbs the radiant

heat thus promoting rapid chemical reactions. The ZIRRUS reactor is a scaled up version (100 kW) of the ROCA reactor (10 kW).

Rotary Kiln

The basic design of rotary kilns, as a hollow cylinder axially rotating heated on one end and fed into on the other, has been applied for decades in numerous applications such as high temperature waste treatment, re-melting of aluminium, refractories, and cement/lime production, amongst others [21,34]. Few applications of solar thermochemical rotary kilns include thermal reduction of Co_3O_4 at the solar furnace of German Aerospace Center (DLR), Cologne and solar calcination of $CaCO_3$ done by ETH, PSI and Qualical [14,21]. The main advantages of rotary kilns are as follows: good heat transfer between gas and solid phase reactions, allowing a high mass flowrate of reactant and high reactive surface area; Maintains low radiation heat loss and obtains a uniform temperature distribution inside the walls; Allows direct irradiation from the reactive material due to the cavity being enclosed by a clear window on one end; Amplifies the heat and mass transfer of the reactive material inside the cavity as well as reducing the sintering of particles, by rotation of the reactor; Continuous mode of operation is possible given a suitable chemical process.

An experimental study conducted by ETH, PSI and QualiCal used a 10 kW solar heated rotary kiln for solar calcination of $CaCO_3$. They demonstrated that solar calcination is indeed feasible [14]. Furthermore, their rotary kiln supported more than 100 h at temperatures up to 1500 K, withstanding the thermal shocks. Above 1500 K, the refractory liner had a minor crack, due to insufficient lining thickness according to Meier et al. [14]. This reactor was also used to calcify $MgCO_3$. Based on this experimental proof of concept, other carbonate chemistries can be calcified in this type of rotary kiln at temperatures close to 1500 K, such as $SrCO_3$.

German Aerospace Center (DLR) and General Atomics performed a case-study on Co_3O_4 redox potential for thermochemical storage using a solar heated rotary kiln. A laboratory scale rotary kiln was designed using a radius-to-length ratio of 1:5 with siliconized silicon carbide as the construction material [21]. Another case-study on solar production of lime using a rotary kiln tests a radius-to-length ratio of 1:3.4 with refractory liners and a stainless steel outer shell casing [14].

Fluidized Bed Reactor

Common in industrial applications, a fluidized bed reactor operates on the underlying concept of fluidizing solid particles as an upward-flowing gas overcomes the particles' gravitational and drag forces. This is most commonly addressed in terms of fluid velocity with respect to particle size distribution. Geldart [20] provides a convenient classification system for powders based on mean particle diameter and bulk fluid density to predict the fluidization characteristics. This information can be used to determine the type of fluidization expected and the calculations that must be executed to design a fluidized bed reactor.

There are several types of fluidized bed reactor designs that differ based on Geldart classification and the fluidization velocity [20,62]. Among them, bubbling fluidized bed (BFB) and circulating fluidized bed (CFB) reactors have potential for solar thermal application. A CFB reactor provides a greater fluid velocity and allows the high temperature solid particles to circulate the entire reactor, increasing mixing efficiency and heat transfer between the solids and gas. Conventional fluidized bed reactors are of BFB type. The commercial vendor Alstom has sold many CFB reactors to coal-fired power generation plants for decreasing air pollutant emissions. Furthermore, heat transfer within a CFB reactor occurs between particles, particle and gas, as well as gas-solid suspension and heat transfer surfaces [63].

Appendix B. Review and Evaluation of Reversible CO_2 Storage Technologies

Literature Review

Reversible CO_2 storage has been studied for purposes of carbon capture. In a review done by Li et al. [64], they conclude that although monoethanolamine (MEA), a commonly used amine-based scrubbing solvent, has a high capacity for CO_2 adsorption, there remains numerous disadvantages. These disadvantages include the sensitivity of MEA to water exposure (entailing an additional drying process), the increase in energy demand and operating cost with the evaporation of water, and the harm of the degradation products to both the environment and human health [64]. However, when combined with amyloid fibers, CO_2 capture stability advantages arise. The adsorption capacity of an MEA solution is roughly 3 mmol cm^{-3}, while the MEA amyloid fiber has an adsorption capacity of 0.6 mmol cm^{-3} [65]. The amyloid fibers exhibit favorable properties when compared to an MEA solution. According to Li et al. [64], when MEA is prepared with amyloid fibers, the solid material exhibits the following favorable properties: potential compatibility with the presence of water, comparatively low regeneration energy requirement, and potential biodegradable characteristics with minimal effect to the environment. With solely an MEA solution, Li et al. [64], states that the energy required for MEA regeneration compared to the energy output of a typical power plant is estimated to be 30%, a value far too high for practical purposes. Considering the improvements made in the capabilities of utilizing MEA as a supporting method for CO_2 capture and storage, MEA amyloid fibers must be further researched.

In an article studying metal-organic frameworks for the capture of CO_2, Fracaroli et al. [66] promote metal-organic frameworks (MOFs) as a superior option to MEA solutions. Fracaroli et al. [66] compare MOFs to MEA solutions stating that the MOFs have adjustable chemical functionality, structural diversity, and ease of functionalization while MEA solutions do indeed present a high energy penalty and environmental hazard. Fracaroli et al. [66] tested the CO_2 capture abilities of MOFs in the presence of water and achieved selective capture in 65% humidity, though they note that such abilities without degradation of performance is uncommon. They introduce an MOF composed of magnesium oxide rods joined by terphenylene organic linkers and functionalized with CH_2NH_2 (IRMOF-74-III–CH_2NH_2), which provides a CO_2 adsorption capacity of 0.8 mmol g^{-1} with successful regeneration. Given the lack of degradation of the MOF structure throughout the CO_2 capture process, MOFs are intriguing. However, in a study on activated carbons for CO_2 capture, Wickramaratne and Jaroniec [25] state that although MOFs exhibit high CO_2 adsorption capacities, e.g. 8.5 mmol g^{-1} by Yazaydin et al. [51], MOFs are very expensive compared to a majority of CO_2 adsorbents, with a cost of roughly 10.6 USD per gram of MOF according to Sigma Aldrich. Wickramaratne and Jaroniec [25] further compared activated carbon to MOFs presenting the following advantages of activated carbons over MOFS: higher resistance to water, higher thermal stability, good chemical resistance to media, and low energy requirements for regeneration.

Alkali metal carbonate solid sorbents have been reviewed by Li et al. [64]. The K-based sorbents were developed and analyzed with various supports. In the review, it was shown that K_2CO_3 supported with activated carbon had an adsorption capacity of 1.95 mmol CO2 g^{-1} sorbent. K_2CO_3 supported with MgO had an even higher adsorption capacity of 2.98 mmol CO_2 g^{-1} sorbent. Both sorbents

reached such capacities at the temperature of 60 °C. Li et al. [64] advocates for these K-based sorbents with their high mechanical strength and good stability over multiple cycles. However, a heat of adsorption estimate of K_2CO_3/AC and K_2CO_3/MgO were higher than desirable, having values of 141.4 KJ mol-sorbent^{-1} and 235.8 KJ mol-sorbent^{-1}, respectively. With such high energy inputs required, these sorbents are impractical to include in a CO_2 absorption and regeneration process.

Sorbent Cost Analysis for Scheme 2

In order to meet DOE SunShot goals, a maximum of \$15 kWh_{th}^{-1} for the solar energy subsystem must be met. This cost limit is all encompassing, including costs for energy storage, heat exchangers, reactors, etc. That may be necessary in the system design. Thus, a value much lower than \$15 kWh_{th}^{-1} must be set as a limit for the CO_2 storage mechanism alone. With reversible CO_2 storage, factors such as tank cost and thermochemical storage material cost are included. The energy required for CO_2 release (heat of adsorption), is also considered when comparing the various reversible CO_2 storage methods. Data for storage capacity at atmospheric pressure has been compiled and compared for various options including ionic liquids, amines, and activated carbons, amongst others.

Direct costs for a number of compounds and materials were frequently unavailable during evaluation. Thus, estimates have been made to conduct an effective cost comparison. Bulk quantity costs for chemicals were obtained through chemical vendors that provide commercial bulk pricing online, such as Sigma Aldrich. In the event that a bulk price was not available, a cost-scaling factor was applied. For compounds with similar molar masses, the costs of the compounds were averaged when necessary, in order to calculate a unit price. All tank costs were calculated using the Towler and Sinnott [32] tank cost calculator for gas storage tanks and the required volume of CO_2 storage material calculated. Depending on the requirements of the evaluated sorbent, either a carbon steel (CS) or stainless steel (SS) tank was considered, with internal linings if necessary. Designing for an 800MWh_{th} storage system, the sum of the tank cost and material cost for each method was divide by the following difference for a conservative estimate: (8×10^5 -internal consumption) kWh, to provide a normalized capital cost for base comparison. The internal consumption accounts for compression work and other autonomous energy consumption such as energy consumed by mechanical parts within the thermochemical energy storage block. It must be noted that this further causes final cost estimates to be highly conservative when presented on a USD per kWh_{th} basis.

The amine PZ/DETA/H_2O has been studied and test for CO_2 absorption. A relatively high CO_2 absorption capacity of 11.6 mmol CO_2 cm^{-3} was achieved by Lin et al., [28]. The unit price per gram of amine is competitive compared to other CO_2 absorption chemistries, with a calculated cost per kWh_{th} of \$4.68, yet not low enough for large-scale CO_2 storage. Furthermore, it has been reported that most amines of this type typically have high regeneration energy penalties [67].

Activated carbon is a commercially available material for CO_2 adsorption. Thus, two activated carbons with high adsorption capacities were analyzed at varying temperatures, specifically CS-6-CD-4 and CS-6-CD-8. Wickramaratne and Jaroniec [25] synthesized monodisperse carbon spheres under various activation hours and carbonization temperatures. The adsorption capacities of the activated carbon spheres show very promising results ranging from 4.4 mmol CO_2 g^{-1} sorbent to 8.05 mmol CO_2 g^{-1} sorbent [25]. In the notation of CS-6-CD-8, the CD notates carbon spheres, the 6 represents the 600 °C carbonization temperature, CD refers to the activation gas of carbon dioxide, and 8 is the activation time in hours. The notation of CS-6-CD-4 follows the same logic. Both activated carbons were analyzed at 0 °C and 25 °C. At lower temperatures, the activated carbons have higher adsorption capacities varying from 5.11 mmol CO_2 cm^{-3} at 25 °C to 8.40 mmol CO_2 cm^{-3} at 0 °C for AC CS-6-CD-4. AC CS-6-CD-8 has an even higher change in adsorption, increasing from 3.93 mmol CO_2 cm^{-3} at 25 °C to 7.19 mmol CO_2 cm^{-3} at 0 °C. A standard cost for activated carbon at bulk price was used to estimate final price, setting carbon steel as the tank material. The activated carbons at 0 °C resulted in competitive prices of \$4.32 per kWh_{th} for CS-6-CD-4 and \$4.08 per kWh_{th} for CS-6-CD-8. Additionally, the activated carbons have attractively low heats of adsorption ranging from 20.3 to 27.7 kJ/mol [25].

Ionic liquids have also been studied for reversible CO_2 absorption [26,53,68–71]. Amongst the numerous ionic liquids in the literature, the most attractive ionic liquid for this application is the cation Choline with an amino acid anion *p*-Methoxyphenolate ([Cho][*p*-methoxy-PhO]). The absorption capacity of [Cho][*p*-methoxy-PhO] is 4.04 mmol CO_2 cm^{-3} at 1 bar and 30 °C [40]. The unit price of the ionic liquid is much less than the other compounds reviewed for CO_2 adsorption. [Cho][*p*-methoxy-PhO] has a considerably low unit price of 0.043 cents per gram, resulting in a normalized cost of \$2.73 per kWh_{th}.

Table B.1

Substance	mmol of CO[b] per cm3 of substance	(P[a],T)	Substance		Energy Density (kWh_{th}/m^3)	q_R (kJ/mol)	T_R	Tank Material[b]	Tank Cost (\$ kWh_{th}^{-1})	Total Cost (\$$kWh_{th}^{-1}$)
			Unit Price (USD/kg)	Cost (\$ kWh_{th}^{-1})						
[Cho][p-methoxy-PhO] [25,26]	4.047	(1, 30 °C)	\$0.43	\$2.15	263.16	19.1 –89.9	–	CS	\$0.58	\$2.14
DES ChCl:Gly:SB [27]	8.516	(1, 25 °C)	\$4.37	\$2.81	551.72	–	–	CS	\$0.35	\$2.47
AC CS-6-CD-8 [25]	7.188	(1, 0 °C)	\$1.93	\$3.69	467.84	22.9 –26.5	0 °C	CS	\$0.39	\$3.19
AC CS-6-CD-4 [25]	8.405	(1, 0 °C)	\$1.93	\$3.96	547.95	20.3 –27.7	0 °C	CS	\$0.35	\$3.37
Amine PZ/DETA/H_20 [28]	11.6	(-, 50 °C)	\$3.75	\$4.26	754.72	145.02	120 °C	SS	\$0.43	\$3.67
Sorbent K_2CO_3/MgO [29]	8.955	(1, 60 °C)	\$0.87	\$4.46	583.94	236	400 °C	CS	\$0.34	\$3.75
Amine PZ/DETA/MeOH/H_2O [28]	9.04	(-, 30 °C)	\$2.66	\$4.51	588.24	102	120 °C	SS	\$0.50	\$3.92
AC CS-6-CD-4 [25]	5.112	(1, 25 °C)	\$1.93	\$6.53	331.95	20.3 –27.7	25 °C	CS	\$0.50	\$5.49
AC CS-6-CD-8 [25]	3.929	(1, 25 °C)	\$1.93	\$6.74	255.59		25 °C	CS	\$0.60	\$5.73

Table B.1 (*continued*)

Substance	mmol of CO[b] per cm3 of substance	(P[a],T)	Substance		Energy Density (kWh_{th}/m^3)	q_R (kJ/mol)	T_R	Tank Material[b]	Tank Cost ($\$ kWh_{th}^{-1}$)	Total Cost ($\$kWh_{th}^{-1}$)
			Unit Price (USD/kg)	Cost ($\$ kWh_{th}^{-1}$)						
						22.9 −26.5				
Sorbent K_2CO_3/AC [29,30]	4.319	(1, 60 °C)	$1.40	$11.08	280.70	89.5	150 °C	CS	$0.56	$9.10
$Ba_4Sb_2O_9$ [31]	8.722	(-, 600 °C)	$2.22	$15.00	567.38	156	950 °C	Alumina	$3.83	$14.72
Gas	0.041	(1, 25 °C)	$0.00	$0.00	0.59	N/A		CS	$31.75	$225.35
Pressurized Gas	0.822	(25, 25 °C)	$0.00	$0.00	14.67	N/A		CS	$92.07	$66.79
Solid	35.492	(1, −78.5 °C)	$0.00	$0.00	2305.48	N/A		CS	$0.16	$0.13

[a] In units of bar.
[b] CS is for Carbon Steel; SS is for Stainless Steel.

Appendix C. Cost and design calculations of subsystem components

Rotary Kiln (Direct Contact Dryer)

The steel casing thickness (t_H or t_L) is a function of the internal pressure (P_{int}), radius (r_{int}), allowable stress (σ) for 316 steel as a function of pressure and temperature, and weld joint efficiency (n_{wj}). Two values for thickness are calculated, one that is a function of hoop stress (t_H) and one that is a function of longitudinal stress (t_L), as shown in Eqs. (C.2) and (C.3). The greater of the two is used in cost calculations. In all calculations, n_{wj} is assumed to be 1.0 following ASME code for pressure vessels.

$$t_H = \frac{P_{int} 2 r_{int}}{2 \times \sigma \times n_{wj} - 1.2 P_{internal}} \tag{C.1}$$

$$t_L = \frac{P_{internal} 2 r_{internal}}{4 \times \sigma \times n_{wj} + 0.8 P_{internal}} \tag{C.2}$$

The resulting thickness of the steel casing is 10 cm. Following experimental demonstrations of solar rotary kilns for thermochemical decomposition, a length-to-radius ratio of 5 is chosen [21].

The following cost correlation was used, specific to a carbon steel direct contact rotary kiln

$$C = -7,400 + 4,350 S^{0.9} \tag{C.3}$$

$$IF = 2.46 \tag{C.4}$$

In which S is the internal surface area of the kiln. It must be noted that the above calculations for solar rotary kilns is preliminary and solely for the purpose of providing rough cost estimates of the solar TCES subsystem.

High Temperature Solids Storage Tank Design

As the cone-roof tank proved less expensive compared to a floating roof tank, cost estimates for the cone-roof tank are presented. For preliminary costing, a 316 stainless steel tank with internal refractory lining is considered. Simple cost installation factors account for insulation without the need for heat transfer calculations to determine the thickness of the lining.

Heat Exchanger

The required surface area of the heat exchanger (A_{HX}) was calculated beginning with Equation (C.5).

$$Q = \dot{m}_{CO2} \int_{T_{H,in}}^{T_{H,out}} C_P \, dT = UA_{HX} \bullet T \tag{C.5}$$

In Eq. (5), the rate of heat transfer Q is expressed as the product of the mass flowrate $\dot{m}_{CO_2}$ and the integral of the heat capacity C_P, of CO_2 over the temperature from the inlet ($T_{H,in} = 1235°C$) to the outlet ($T_{H,out} = 25°C$) of the heat exchanger. The rate of heat transfer can also be expressed as the product of overall the heat transfer coefficient U, the area over which heat transfer occurs A_{HX} and the temperature difference ΔT. Solving Eq. (5) for the area results in

$$A_{HX} = \dot{m}_{CO2} \frac{\int_{T_{H,in}}^{T_{H,out}} C_P \, dT}{U \cdot T} \tag{C.6}$$

The mass flowrate of CO_2 from the rotary kiln for the imposed design parameter of 100 MWth can be calculated using reaction stoichiometry and input feed molar flowrate. Given an input feed molar flowrate of 855 mol/s for a 50% reaction rate, $\dot{m}_{CO_2}$ is hence ~38 kg/s. Typical values for the overall heat transfer coefficient U for a gas-gas HX under forced convection typically ranges between 10 and 30 $W\,m^{-2}K^{-1}$, for which an average value of 20 $W\,m^{-2}K^{-1}$ is considered [72]. This results in an area of ~1200 m^2.

With a low temperature heat exchanger, the heat released will result in lower efficiencies. However, with a high temperature heat exchanger, the cost per kWh_{th} will exceed the limit DOE has set once other costs are added. Comparisons of cost for a high temperature heat exchanger versus the effects of heat loss with a low temperature heat exchanger must be performed before concluding with an optimal heat exchanger design.

Compressor

Under the conditions of isentropic compression, the volume of CO_2 in the final state (V_2) can be determined as.

$$V_2 = \left(\frac{P_1 V_1^k}{P_2} \right)^{\frac{1}{k}} \tag{C.7}$$

where k is c_p/c_v, P_1 and P_2 are the initial and final CO_2 pressure, respectively, and V_1 is the initial volume calculated using the ideal gas law. Similarly, the temperature at the outlet of the compressor can be calculated as

$$\frac{T_2}{T_1} = \left(\frac{P_2}{P_1} \right)^{\frac{k-1}{k}} \tag{C.8}$$

Cost Breakdown

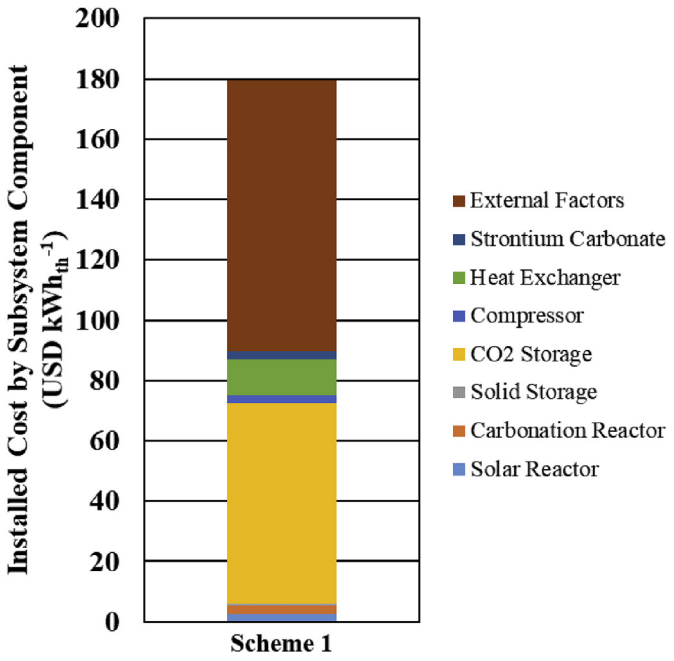

Fig. C.1. Bar graph of Scheme 1 cost breakdown. It is clear that the main cost contributing components are the CO_2 storage method and external factors such as installation, delivery, and other parameters included in the calculation of IF.

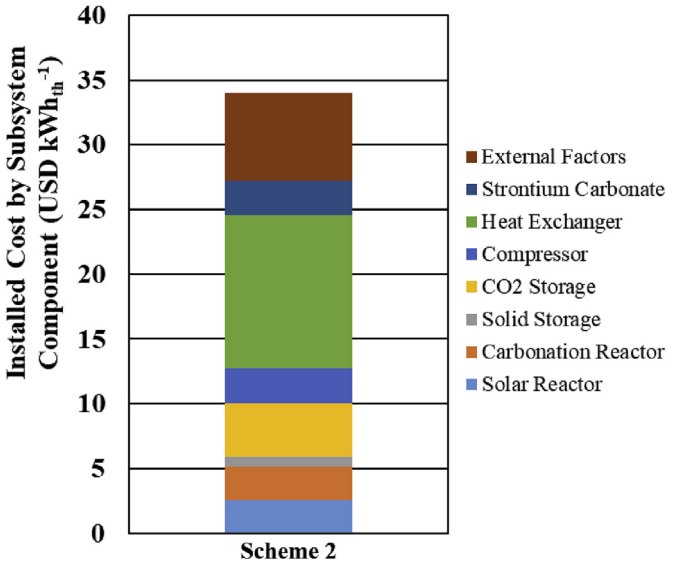

Fig. C.2. Bar graph of Scheme 2 cost breakdown. Like Scheme 1, the main cost contributing components are the heat exchange and external factors such as installation and delivery. Unlike Scheme 1, costs are more sensitive to other components such as the high temperature heat exchanger, due to the overall reduced capital cost resultant of the less expensive CO_2 storage method.

Estimate of Operations and Maintenance Cost

The cost of fixed operations and maintenance (O&M) for each subsystem Scheme must be rigorously calculated for a fair overall evaluation of the subsystem economics, due to the significant contribution they make towards the total cost of the system. An isolated cost of O&M for thermal energy storage systems are not available, rather estimates for a CSP plant with thermal energy storage are more prevalent. Though much of the literature simply estimates O&M as 1–2.5% of total capital cost, the true O&M cost may be higher after taking all details into consideration [73–75]. The total O&M cost estimate for Scheme 1 and Scheme 2 encompasses the following costs based on typical chemical plant design assumptions, with corresponding values presented in Table S2 [32].

The Inside Battery Limits (ISBL) capital cost includes the direct and indirect field costs, equipment, and installation costs of the TCES subsystem, which is approximately that of the total installed capital cost (TCC) once installation factors are included. Then, the outside battery limits (OSBL) cost can be estimated as 40% of the ISBL. The estimated O&M cost includes incurred cost of property taxes and insurance which is estimated as 1% of the TCC. It is further assumed that the land upon which the TCES is constructed has been rented rather purchased, hence leading to a rent of land fee (1% of the sum of TCC and OSBL).

To calculate operating labor cost (OLC), it is assumed that 15 operators are required; five crews of 3 operators/shift in alternating schedules to account for a plant operating 24 h per day, 7 days a week. An average operator salary of 50,000 USD per shift position per year is considered in the cost of operating labor, with a single shift position equivalent to 4.8 operators. Relative to the operating labor, supervision and direct salary overhead are also included in cost of O&M. The cost for supervision is estimated as 25% of the OLC while direct salary overhead (DSO) is estimated as 50% of the sum of OLC and supervision cost.

Maintenance cost includes that of required materials and labor, and is assumed to account for material cost of $SrCO_3$. Here, maintenance cost is assumed to be 4% of the TCC. Future work must be done to determine the long-term cyclability of $SrCO_3$ to accurately evaluate annual material cost. Total O&M cost further includes the general plant overhead that accounts for research and development of the subsystem, human resources, sales and marketing, etc. Which can be estimated as 65% of the sum of supervision cost, DSO, and maintenance cost.

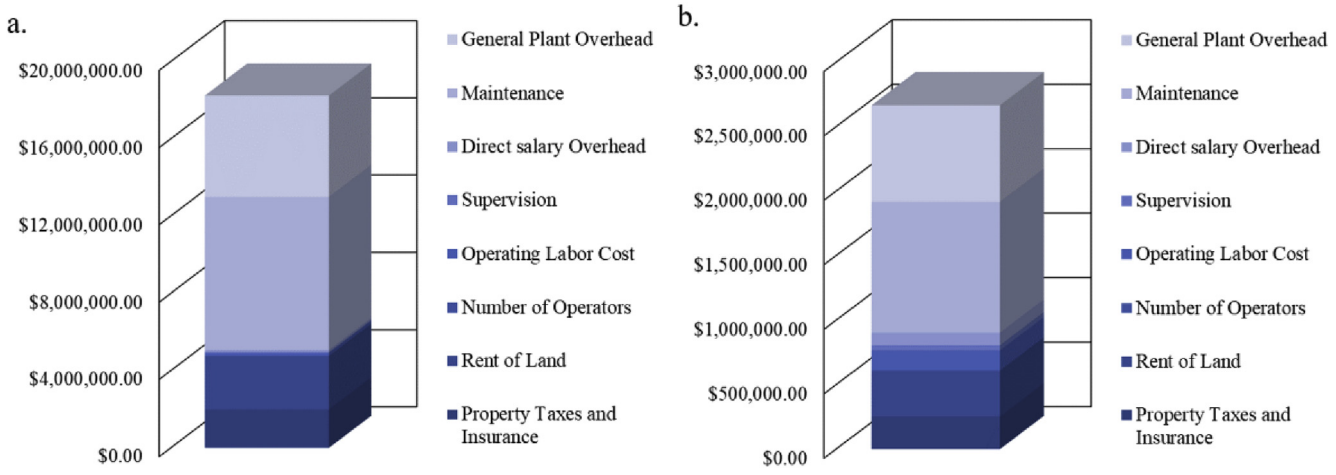

Fig. C.3. Operations and Maintenance cost breakdown for Scheme 1 (a) and Scheme 2 (b).

As expected by the higher capital cost, Scheme 1 has a significantly higher O&M cost of ~23 USD kWh_{th}^{-1} per year compared to Scheme 2 which has an O&M cost of ~3 USD kWh_{th}^{-1} per year.

Table C.1
Detailed Calculation of O & M Cost for Scheme 1 and Scheme 2.

	Calculation Method [32]	Scheme 1	Scheme 2
TCC	Refer to Main Text	198 MMUSD	25 MMUSD
OSBL	40% of TCC	79 MMUSD	10 MMUSD
Property Taxes and Insurance	1% of TCC	1.975 MMUSD yr^{-1}	245,000 USD yr^{-1}
Rent of Land	1% of (TCC + OSBL)	2.765 MMUSD yr^{-1}	343,000 USD yr^{-1}
Operating Labor Cost (OLC)	15 operators	156,250 USD yr^{-1}	156,250 USD yr^{-1}
Supervision	25% of OLC	39,000 USD yr^{-1}	39,000 USD yr^{-1}
Direct Salary Overhead (DSO)	50% of (OLC + Supervision)	97,650 USD yr^{-1}	97,650 USD yr^{-1}
Maintenance	4% of TCC	7.9 MMUSD yr^{-1}	980,000 USD yr^{-1}
General Plant Overhead	65% of (Supervision + DSO + Maintenance)	5.22 MMUSD yr^{-1}	725,900 USD yr^{-1}
	Total O & M Cost = Σ	**18.2 MMUSD yr^{-1}**	**2.59 MMUSD yr^{-1}**

References

[1] IEA, Medium-term Market Report, 2015.
[2] EERE. Concentrating Solar Power: Efficiently Leveraging Equilibrium Mechanisms for Engineering New Thermochemical Storage n.d. https://www1.eere.energy.gov/financing/solicitations_detail.html?sol_id=602 (accessed December 2, 2016).
[3] S. Kuravi, J. Trahan, D.Y. Goswami, M.M. Rahman, E.K. Stefanakos, Thermal energy storage technologies and systems for concentrating solar power plants, Prog. Energy Combust. Sci. 39 (2013) 285–319, https://doi.org/10.1016/j.pecs.2013.02.001.
[4] E. Fletcher, R. Moen, Hydrogen- and oxygen from water, Science 197 (1977) 1050–1056.
[5] A. Steinfeld, Solar thermochemical production of hydrogen - a review, Sol. Energy 78 (2005) 603–615, https://doi.org/10.1016/j.solener.2003.12.012.
[6] Hartung L. Predicting Radiative Heat Transfer in Thermochemical Nonequilibrium Flow Theory Manual for the LORAN Code n.d.
[7] W. Lipinski, D. Thommen, A. Steinfeld, Unsteady radiative heat transfer within a suspension of ZnO particles undergoing thermal dissociation, Chem. Eng. Sci. 61 (2006) 7029–7035, https://doi.org/10.1016/j.ces.2006.07.037.
[8] S. Ströhle, A. Haselbacher, Z.R. Jovanovic, A. Steinfeld, The effect of the gas-solid contacting pattern in a high-temperature thermochemical energy storage on the performance of a concentrated solar power plant, Energy Environ. Sci. (2016), https://doi.org/10.1039/C5EE03204K.
[9] T. Block, M. Schmücker, Metal oxides for thermochemical energy storage: a comparison of several metal oxide systems, Sol. Energy 126 (2016) 195–207.
[10] C. Corgnale, B. Hardy, T. Motyka, R. Zidan, J. Teprovich, B. Peters, Screening analysis of metal hydride based thermal energy storage systems for concentrating solar power plants, Renew. Sustain. Energy Rev. 38 (2014) 821–833. https://doi.org/10.1016/j.rser.2014.07.049.
[11] K. Lovegrove, W. Stein, Concentrating Solar Power Technology - Principles, Developments and Applications, vol. 21, 2012.
[12] T. Yan, R.Z.Z. Wang, T.X.X. Li, L.W.W. Wang, I.T. Fred, A review of promising candidate reactions for chemical heat storage, Renew. Sustain. Energy Rev. 43 (2015) 13–31, https://doi.org/10.1016/j.rser.2014.11.015.
[13] M. Felderhoff, R. Urbanczyk, S. Peil, Thermochemical heat storage for high temperature applications-A review, Green 3 (2013) 113–123, https://doi.org/10.1515/green-2013-0011.
[14] A. Meier, E. Bonaldi, G.M. Cella, W. Lipinski, D. Wuillemin, R. Palumbo, Design and experimental investigation of a horizontal rotary reactor for the solar thermal production of lime, Energy 29 (2004) 811–821. https://doi.org/10.1016/S0360-5442(03)00187-7.
[15] P. Pardo, a. Deydier, Z. Anxionnaz-Minvielle, S. Rougé, M. Cabassud, P. Cognet, A review on high temperature thermochemical heat energy storage, Renew. Sustain. Energy Rev. 32 (2014) 591–610, https://doi.org/10.1016/j.rser.2013.12.014.
[16] N.R. Rhodes, A. Barde, K. Randhir, L. Li, D.W. Hahn, R. Mei, et al., Solar thermochemical energy storage through carbonation cycles of SrCO $_3$/SrO supported on SrZrO $_3$, ChemSusChem (2015), https://doi.org/10.1002/cssc.201501023 n/a-n/a.
[17] A.C. Tuck, USGS Minerals Resources Program 2016, 2016.
[18] B.T.R. Yager, H.R. Newman, Minerals Yearbook 2014, 2012.
[19] a. C. Hoffmann, Introduction to fluidization, Chem. Eng. Sci. 24 (1986) 119–126.
[20] D. Geldart, Types of gas fluidization, Powder Technol. 7 (1973) 285–292, https://doi.org/10.1016/0032-5910(73)80037-3.
[21] M. Neises, S. Tescari, L. de Oliveira, M. Roeb, C. Sattler, B. Wong, Solar-heated rotary kiln for thermochemical energy storage, Sol. Energy 86 (2012) 3040–3048, https://doi.org/10.1016/j.solener.2012.07.012.
[22] A. Meier, E. Bonaldi, G.M. Cella, W. Lipinski, Multitube rotary kiln for the industrial solar production of lime, J. Sol. Energy Eng. 127 (2005) 386–395.
[23] S.M. Benson, D.C. Thomas (Eds.), Carbon Dioxide Capture for Storage in Deep Geologic Formations-results from the CO2 Capture Project, first ed., Elsevier Science, 2005.
[24] E. Bagherisereshki, J. Tran, F. Lei, N. AuYeung, Investigation into SrO/SrCO3 for high temperature thermochemical energy storage, Sol. Energy 160 (2018) 85–93, https://doi.org/10.1016/J.SOLENER.2017.11.073.
[25] N.P. Wickramaratne, M. Jaroniec, Activated carbon spheres for CO2

adsorption, ACS Appl. Mater. Interfaces 5 (2013) 1849–1855, https://doi.org/10.1021/Am400112m.
[26] C. Wang, X. Luo, X. Zhu, G. Cui, D. Jiang, D. Deng, et al., The strategies for improving carbon dioxide chemisorption by functionalized ionic liquids, RSC Adv. 3 (2013) 15518, https://doi.org/10.1039/c3ra42366b.
[27] L.L. Sze, S. Pandey, S. Ravula, S. Pandey, H. Zhao, G a Baker, et al., Ternary deep eutectic solvents tasked for carbon dioxide capture, ACS Sustain. Chem. Eng. (2014), https://doi.org/10.1021/sc5001594. Ahead of Print.
[28] P.-H. Lin, D.S.H. Wong, Carbon dioxide capture and regeneration with amine/alcohol/water blends, Int. J. Greenh. Gas Contr. 26 (2014) 69–75, https://doi.org/10.1016/j.ijggc.2014.04.020.
[29] S.C. Lee, B.Y. Choi, T.J. Lee, C.K. Ryu, Y.S. Ahn, J.C. Kim, CO2 absorption and regeneration of alkali metal-based solid sorbents, Catal. Today 111 (2006) 385–390. https://doi.org/10.1016/j.cattod.2005.10.051.
[30] N. Shigemoto, T. Yanagihara, S. Sugiyama, H. Hayashi, Material balance and energy consumption for CO2 recovery from moist flue gas employing K2CO3-on-Activated carbon and its evaluation for practical adaptation, Energy Fuel. 20 (2006) 721–726, https://doi.org/10.1021/ef058027x.
[31] M.T. Dunstan, W. Liu, A.F. Pavan, J.A. Kimpton, C.D. Ling, S.A. Scott, et al., Reversible CO 2 Absorption by the 6H Perovskite Ba 4 Sb 2 O 9, 2013, p. 4891.
[32] G. Towler, R. Sinnott, Chemical Engineering Design, second ed., 2012.
[33] S. Tescari, C. Agrafiotis, S. Breuer, L. de Oliveira, M.N. Puttkamer, M. Roeb, et al., Thermochemical solar energy storage via redox oxides: materials and reactor/heat exchanger concepts, Energy Proc. 49 (2014) 1034–1043, https://doi.org/10.1016/j.egypro.2014.03.111.
[34] S. Tescari, M. Neises, L. de Oliveira, M. Roeb, C. Sattler, P. Neveu, Thermal model for the optimization of a solar rotary kiln to be used as high temperature thermochemical reactor, Sol. Energy 95 (2013) 279–289, https://doi.org/10.1016/j.solener.2013.06.021.
[35] W.L. McCabe, H.P. Smith, Unit Operations of Chemical Engineering, McGraw-Hill, 2001.
[36] R.K. Shah, D.R. Sekulib, CHAPTER 17 HEAT EXCHANGERS, Handb. Heat Transf. 3 (1998).
[37] T. Yager, Minerals Yearbook: Malawi 2015, 2013.
[38] U. Herrmann, B. Kelly, H. Price, Two-tank molten salt storage for parabolic trough solar power plants, Energy 29 (2004) 883–893, https://doi.org/10.1016/S0360-5442(03)00193-2.
[39] A. Luzzi, K. Lovegrove, E. Filippi, H. Fricker, M. Schmitz-goeb, M. Chandapillai, et al., TECHNO-ECONOMIC ANALYSIS OF A 10 MWe SOLAR THERMAL POWER PLANT USING AMMONIA-BASED THERMOCHEMICAL ENERGY STORAGE, Sol. Energy 66 (1999) 91–101, https://doi.org/10.1016/S0038-092X(98)00108-X.
[40] P. Sanglard, O. Vorlet, R. Marti, O. Naef, E. Vanoli, CO2 capture by ionic liquids – an answer to anthropogenic CO2 emissions? Chim. Int. J. Chem. 67 (2013) 711–718, https://doi.org/10.2533/chimia.2013.711.
[41] J.F. Brennecke, B.E. Gurkan, Ionic liquids for CO $_2$ capture and emission reduction, J. Phys. Chem. Lett. 1 (2010) 3459–3464, https://doi.org/10.1021/jz1014828.
[42] H. Chen, C. Zhao, Y. Li, X. Chen, CO2 capture performance of calcium-based sorbents in a pressurized carbonation/calcination loop, Energy Fuel. 24 (2010) 5751–5756, https://doi.org/10.1021/ef100565d.
[43] A.M. Kierzkowska, R. Pacciani, C.R. Müller, CaO-based CO2 sorbents: from fundamentals to the development of new, highly effective materials, ChemSusChem 6 (2013) 1130–1148, https://doi.org/10.1002/cssc.201300178.
[44] W. Liu, B. Feng, Y. Wu, G. Wang, J. Barry, J.C.D. da Costa, Synthesis of sintering-resistant sorbents for CO2 capture, Environ. Sci. Technol. 44 (2010) 3093–3097, https://doi.org/10.1021/es903436v.
[45] E.S. Rubin, A.B. Rao, C. Chen, A.B. Rao, Cost and performance of fossil fuel power plants with CO2 capture and storage, Energy Pol. 35 (2007) 4444–4454, https://doi.org/10.1016/j.enpol.2007.03.009.
[46] S. Himeno, T. Komatsu, S. Fujita, High-pressure adsorption equilibria of methane and carbon dioxide on several activated carbons, J. Chem. Eng. Data 50 (2005) 369–376, https://doi.org/10.1021/je049786x.
[47] U.S. Energy Information Administration, International Energy Outlook 2016, 2016.
[48] P. Riemer, Greenhouse gas mitigation technologies, an overview of the CO 2 capture, storage and future activities of the IEA greenhouse gas R&D programme, Energy Convers. Manag. 37 (1996) 665–670.
[49] P. Freund, Making deep reductions in CO2 emissions from coal-fired power plant using capture and storage of CO2, Proc. Inst. Mech. Eng. Part A J Power Energy 217 (2003) 1–7.
[50] J. Koornneef, T. van Keulen, A. Faaij, W. Turkenburg, Life cycle assessment of a pulverized coal power plant with post-combustion capture, transport and storage of CO 2, Int. J. Greenh. Gas Contr. 2 (2008) 448–467.
[51] a O. Yazaydin, R.Q. Snurr, T.-H. Park, K. Koh, J. Liu, M.D. Levan, et al., Screening of metal-organic frameworks for carbon dioxide capture from flue gas using a combined experimental and modeling approach, J. Am. Chem. Soc. 131 (2009) 18198–18199, https://doi.org/10.1021/ja9057234.
[52] S. Kumar, S.K. Saxena, A comparative study of CO2 sorption properties for different oxides, Mater. Renew. Sustain. Energy 3 (2014), https://doi.org/10.1007/s40243-014-0030-9.
[53] B.F. Goodrich, J.C. De La Fuente, B.E. Gurkan, D.J. Zadigian, E. a. Price, Y. Huang, et al., Experimental measurements of amine-functionalized anion-tethered ionic liquids with carbon dioxide, Ind. Eng. Chem. Res. 50 (2011) 111–118, https://doi.org/10.1021/ie101688a.
[54] P. Chiesa, E. Macchi, A Thermodynamic Analysis of Different Options to Break 60% Electric Efficiency in Combined Cycle Power Plants, 2002, pp. 987–1002.
[55] C.S. Rajoria, S. Agrawal, A.K. Dash, G.N. Tiwari, M.S. Sodha, A newer approach on cash flow diagram to investigate the effect of energy payback time and earned carbon credits on life cycle cost of different photovoltaic thermal array systems, Sol. Energy 124 (2016) 254–267. https://doi.org/10.1016/j.solener.2015.11.034.
[56] A.H. Abedin, M a Rosen, Closed and open thermochemical energy storage: energy- and exergy-based comparisons, Energy 41 (2012) 83–92, https://doi.org/10.1016/j.energy.2011.06.034.
[57] A. Hepbasli, A key review on exergetic analysis and assessment of renewable energy resources for a sustainable future, Renew. Sustain. Energy Rev. 12 (2008) 593–661, https://doi.org/10.1016/j.rser.2006.10.001.
[58] C.H. Yu, C.H. Huang, C.S. Tan, A review of CO2 capture by absorption and adsorption, Aerosol. Air Qual. Res. 12 (2012) 745–769, https://doi.org/10.4209/aaqr.2012.05.0132.
[59] E. Steiner, J. Ganz, a Meier, M. Sturzenegger, Novel solar reactor for studying ultrafast gas-solid reactions above 2,000 K, AIChE J. 49 (2003) 2937–2947, https://doi.org/10.1002/aic.690491123.
[60] P. Pardo, Z. Anxionnaz-Minvielle, S. Rougé, P. Cognet, M. Cabassud, Ca(OH)2/CaO reversible reaction in a fluidized bed reactor for thermochemical heat storage, Sol. Energy 107 (2014) 605–616, https://doi.org/10.1016/j.solener.2014.06.010.
[61] P. Haueter, S. Moeller, R. Palumbo, a Steinfeld, The production of zinc by thermal dissociation of zinc oxide - solar chemical reactor design, Sol. Energy 67 (1999) 161–167, https://doi.org/10.1016/S0038-092x(00)00037-2.
[62] R. Cocco, S.R. Karri, T. Knowlton, Introduction to Fluidization, 2014, pp. 21–29.
[63] H.M. Abdelmotalib, M. a. M. Youssef, A. a. Hassan, S.B. Youn, I.-T. Im, Heat transfer process in gas–solid fluidized bed combustors: a review, Int. J. Heat Mass Tran. 89 (2015) 567–575, https://doi.org/10.1016/j.ijheatmasstransfer.2015.05.085.
[64] L. Li, N. Zhao, W. Wei, Y. Sun, A review of research progress on CO2 capture, storage, and utilization in Chinese Academy of Sciences, Fuel 108 (2013) 112–130, https://doi.org/10.1016/j.fuel.2011.08.022.
[65] D. Li, H. Furukawa, H. Deng, C. Liu, O.M. Yaghi, D.S. Eisenberg, Designed amyloid fibers as materials for selective carbon dioxide capture, Proc. Natl. Acad. Sci. U. S. A. 111 (2014) 191–196, https://doi.org/10.1073/pnas.1321797111.
[66] A.M. Fracaroli, H. Furukawa, M. Suzuki, M. Dodd, S. Okajima, O.M. Yaghi, Carbon Dioxide Capture in the Presence of Water, 2014, 8863–6.
[67] Lail M, Coleman L, Jamal A, Lesemann M, Gupta R. Novel Non-aqueous CO 2 Solvents and Capture Process with Substantially Reduced Energy Penalties n.d.:1–2.
[68] J. Huang, T. Rüther, Why are ionic liquids attractive for \ce{CO2} absorption? An overview, Aust. J. Chem. 62 (2009) 298, https://doi.org/10.1071/CH08559.
[69] J. Huang, A. Rosamilia, H. Liu, J. Jeffery, Development of Novel Ionic Liquids to Capture CO2 1–26, 2012.
[70] Z. Zhao, H. Dong, X. Zhang, The research progress of CO2 capture with ionic liquids, Chin. J. Chem. Eng. 20 (2012) 120–129, https://doi.org/10.1016/S1004-9541(12)60371-1.
[71] X. Luo, Y. Guo, F. Ding, H. Zhao, G. Cui, H. Li, et al., Significant improvements in CO2 capture by pyridine-containing anion-functionalized ionic liquids through multiple-site cooperative interactions, Angew. Chem. Int. Ed. 53 (2014) 7053–7057, https://doi.org/10.1002/anie.201400957.
[72] J.H. Lienhard, A Heat Transfer Textbook, Fourth, 2013.
[73] J. Hernandez-Moro, J.M. Martinez-Duart, Analytical model for solar PV and CSP electricity costs: present LCOE values and their future evolution, Renew. Sustain. Energy Rev. 20 (2013) 119–132, https://doi.org/10.1016/j.rser.2012.11.082.
[74] P. Viebahn, Final report on technical data, costs, and life cycle inventories of solar thermal power plants, Needs (2008) 1–95.
[75] W. Short, D.J. Packey, A Manual for the Economic Evaluation of Energy Efficiency and Renewable Energy Technologies, 1995.